1-13-2021

Amount and Depositional Fate of Carbon Mobilized by Landsliding in SE Alaska

Bryce Alois Vascik
Portland State University

Amount and Depositional Fate of Carbon Mobilized by Landsliding in SE Alaska

by

Bryce Alois Vascik

A thesis submitted in partial fulfillment of the
requirements for the degree of

Master of Science
In
Geology

Thesis Committee:
Adam M. Booth, Chair
Ashley Streig
John Bershaw
Brian Buma

Portland State University
2020

Abstract

Forest disturbances in the form of landslides mobilize carbon (C) sequestered in vegetation and soils. The mobilized C has two basic depositional fates, deposition onto hillslopes or into water, which sequester C from and release C to the atmosphere at different time scales. The C-dense old-growth temperate forests of SE Alaska are a unique location to quantify the C mobilization rate by frequent landslide events. In this study, we estimate the amount of C mobilized by debris flows over historic time scales by combining a landslide inventory with maps of modeled biomass and soil carbon. We then infer depositional fate over geologic time scales via simulated debris flow deposition modelling with DFLOWZ, calibrated to the study area. In August 2015, a single storm initiated 66 debris flows near Sitka, AK and mobilized 57,651 ± 3,266 tC, while historic storms over a 55-year period in SE Alaska mobilized a total of 4.69 ± 0.21 MtC. Approximately 21% of historic debris flows intersected the stream network, which was consistent with long-term modeled connectivity and suggests that debris flows likely contribute to measured high dissolved organic C in streams and globally significant amounts of C buried in local fjord sediments. Moderate landslide frequency in areas with high C density mobilized C at the highest rates. Our results are consistent with an emerging consensus that disturbances which mobilize organic carbon may play an important role in the global carbon cycle over geologic time, in addition to geochemical processes such as silicate weathering.

Acknowledgments

This project received funding from NSF Award EAR-1711986 to Booth. We would like to thank the following field assistants for their contributions: Cora Seibert, Christian Sifford, David de Guzman, Kyle Turchick, and the Sitka Science Center for their hospitality. Carbon models obtained via Brian Buma. The landslide inventory was obtained through the USDA Forestry Service Region 10.

Table of Contents

List of Tables

List of Figures

1. Introduction

Landslides occur on sloped terrain around the world, causing fatalities, damaging property, disrupting infrastructure networks, and altering ecosystems. Regional landslide rates are influenced by climatic and tectonic conditions, with wet climates initiating rainfall-induced landslides and tectonically active areas initiating earthquake triggered landslides. From 2004 to 2016, an estimated 4800 fatalities occurred from rainfall-induced landslides alone, with the most susceptible regions being Central America, South America, east Africa, and Asia (Froude & Petley, 2018). Within the United States, landsliding disrupts infrastructure and can cause fatalities such as the 2014 Oso landslide (Iverson et al., 2015). Landslides also serve as mechanisms for carbon (C) mobilization in densely forested regions that experience a high rate of landsliding by stripping vegetation and soil from hillslopes. Those materials are deposited elsewhere in the landscape or exported to the oceans via river systems (Hilton & West, 2020). If landslide-mobilized carbon is efficiently buried in offshore sediments, landslides may be an important geologic carbon sink, especially if landsliding occurs frequently or with large magnitude events. Landslides are commonly recognized for their destructive potential to infrastructure and livelihoods (Aleotti & Chowdhury, 1999; Alexander, 2005; Fiorillo et al., 2001; Guzzetti et al., 2003), but the amount and depositional fate of carbon transported during landslide triggering events has only been determined for a handful of events around the world (e.g. Clark et al., 2016; Hilton et al., 2011; Madej, 2010; Mohr et al., 2017; West et al., 2011).

Globally, terrestrial ecosystems are estimated to contain $2.76 * 10^{12}$ tC in the form of biomass carbon (C_{bio}) and soil organic carbon (SOC) (Wang et al., 2010). Carbon

distribution throughout terrestrial ecosystems at various spatial and temporal scales has been the focus of many studies due to the important role the terrestrial biosphere plays in the global carbon cycle (Arriaga & Lowery, 2005; Chen et al., 2003; Dixon & Turner, 1991; Hilton 2017; Hilton & West, 2020; Wang et al., 2010). For example, at the global scale, the flux of organic carbon from mountainous landscapes to burial in offshore sediments is likely comparable in magnitude to weathering-related fluxes traditionally thought to control the carbon cycle over geologic time scales (Hilton & West, 2020). If revegetation post-disturbance occurs more rapidly than decay, respiration, and burial of mobilized C, a net loss from the atmospheric carbon pool would result over the relevant decay and revegetation timescales.

Depositional fate, defined here as where carbon is deposited once mobilized, is a primary control on the timescale for sequestration of mobilized carbon (Stallard, 1998). Short-term sequestration of landslide-mobilized carbon occurs through the integration of material into the forest soil, resulting in the accumulation of carbon within the soil organic horizon (Currie et al., 2002). Larger fragments of wood, which we refer to as coarse woody debris (CWD) (> 10 cm diameter), are typically deposited on the soil surface or buried in the debris flow deposit. Residence times for carbon sequestered in soil varies between hundreds of years and several millenniums depending on soil and climatic conditions (Rumpel et al., 2002; Schimel et al., 1994). Climate and moisture are two major controls on respiration rates for CWD, with cold and dry climates reducing respiration, or vice versa (Harmon et al., 1986). In wet and warm climates, respiration can result in up to 76% of carbon transferred to the atmosphere from CWD (Chambers et al., 2001), whereas cooler and drier climates experience relatively lower respiration rates

(Progar et al., 2000; Marra & Edmonds, 1994). Non-respirated carbon is transferred to the depositional zone's soil over years to centuries through leaching (Russell et al., 2015; Wiebe et al., 2014). Higher precipitation has been correlated with increased production of dissolved organic matter through leaching in leaf litter, CWD, and soils (Hafner et al., 2005).

Long-term C sequestration occurs with direct deposition into a body of water, or to a stream that can efficiently export CWD and particulate organic carbon (POC) (0.22 – 0.7 μm) to a body of water. CWD and POC delivered to a body of water allow the potential for burying through sedimentation (Turowski et al., 2016), although some carbon metabolizes and acts as a CO_2 source to the atmosphere during stream transport (Hotchkiss et al., 2016). For example, C_{bio} in the form of CWD can reside within a stream for long periods of time (> 300 years) as decomposition occurs, even though that decomposition occurs relatively slowly compared to surface exposed CWD (Aumen et al., 1983, Chen et al., 2005; Medeiros et al., 2009). However, as some of that CWD is broken down into smaller fragments, fluvial entrainment becomes feasible, and fragments are subsequently carried downstream (Triska & Cromack, 1980). Overall, despite C losses to the atmosphere during stream transport, terrestrial organic matter represents approximately one-third of all buried organic matter within marine sediments globally, and carbon burial efficiency increases with sedimentation rate (Aller, 1998; Burdige, 2005). Coastal mountains exhibit high marine shelf sedimentation due to landslides, which initiate on steep slopes and cause near-instant export of sediment from hillslopes to the ocean (Jaeger et al., 1998; Milliman & Syvitski, 1992). This leads to coastal mountain ranges being a prime location for burial of landslide-mobilized carbon, especially when

the frequency or magnitude of carbon mobilizing events is high (Hilton et al., 2011; West et al., 2011; Frith et al., 2018).

Of the variety of landslides that exist, debris flows in particular pose great risks to life and property due to their increased mobility relative to other landslide types (e.g. Iverson, 1997). Debris flows are moving masses of saturated sediment which often begin as shallow landslides triggered by increasing pore-pressure that reduces the shear strength of soils (Iverson, 1997). Landslides mobilize into debris flows due to high (near lithostatic) pore-pressures and entrain soils and aboveground biomass along their runout paths, commonly incising channels down to bedrock (Iverson et al., 1997; Stock & Dietrich, 2006). Water therefore plays a major role in the initiation of landslides and mobilization of failed sediments into debris flows. In turn, many regions that experience debris flows are vegetated. Entrainment of aboveground biomass (such as tree trunks, branches, and shrubs) commonly occurs, depositing atop previous landslide debris, within stream channels, or on colluvial fans (Lancaster, 2003; May 2002). As velocity slows due to decreasing slope, deposition begins and the active flow volume also decreases until forming a deposit. Where inundation occurs throughout the terrain determines the depositional fate of transported sediment and biomass, which in turn affects carbon sequestration rates and timescales. However, few researchers have examined the quantities and depositional fates of aboveground biomass and soil carbon mobilized by climatic or tectonic events that trigger landslides in North America – a continent in which the terrestrial biosphere plays a major role in global carbon cycling (Fan et al., 1992).

Predicting debris flow inundation is important due to the hazardous implications of fast-moving debris through settlements (Berti and Simoni, 2007; Cui et al., 2011; Iverson et al., 1998; Reid et al., 2016). Most commonly applied methods for predicting debris flow inundation for hazard analysis utilize semi-empirical relationships between a debris flow's volume and runout, such as length or inundated planimetric area (Iverson et al., 1998; Rickenmann, 1999). The introduction of semi-empirical relationships between debris flow volume and inundation area form the basis for geohazard assessment projects in regions that experience debris flows around the world (Iverson et al., 1998; Reid et al., 2016; Scheidl & Rickenmann, 2010). Those assessments often rely on debris flow inundation simulation modeling software that utilizes the semi-empirical relationships, such as LAHARZ (Schilling, 1998) or DFLOWZ (Berti & Simoni, 2007).

Determining the depositional fate of mobilized carbon, the focus of our study, is achievable by coupling landslide inventories with maps of C_{bio} and SOC derived from field measurements and remote sensing data (Clark et al., 2016; Frith et al., 2018; Hilton et al., 2011; West et al., 2011; Wang et al., 2016). That approach has shown that large carbon mobilization events around the world include large-scale intermittent landslide inducing events, such as earthquakes (Frith et al., 2018; Hilton et al., 2011; Wang et al., 2016), storms (Clark et al. 2016; West et al., 2011), and volcanic eruptions (Mohr et al., 2017). For example, in heavily forested mountainous regions, a relatively small debris flow with a volume of 1,000 m^3 can entrain hundreds of metric tons of carbon (Booth et al., 2020; Buma & Johnson, 2015), and large storm events can trigger dozens of debris flows within a single day (Sitka Geotask Force, 2016).

This study estimates the quantity and depositional fate of C_{bio} and SOC mobilized by debris flows in SE Alaska. Three spatial and temporal dimensions will be examined here (Figure 1): (1) a single storm that occurred in August 2015 near Sitka, AK with a footprint of 790-1,103 km^2, (2) multi-decadal carbon mobilization within the larger 70,586 km^2 Tongass National Forest (TNF) in SE Alaska, and (3) modeled post-glacial (~10 ky) time-scales in a representative small 84 km^2 area containing several watersheds near Sitka. At the two shortest temporal scales, the amount of mobilized carbon is estimated by combining mapped landslides with existing maps of carbon density. The depositional fate of mobilized carbon for all three spatio-temporal scales is determined by estimating the percent of mapped or modeled debris flows which deposited materials on hillslopes versus streams.

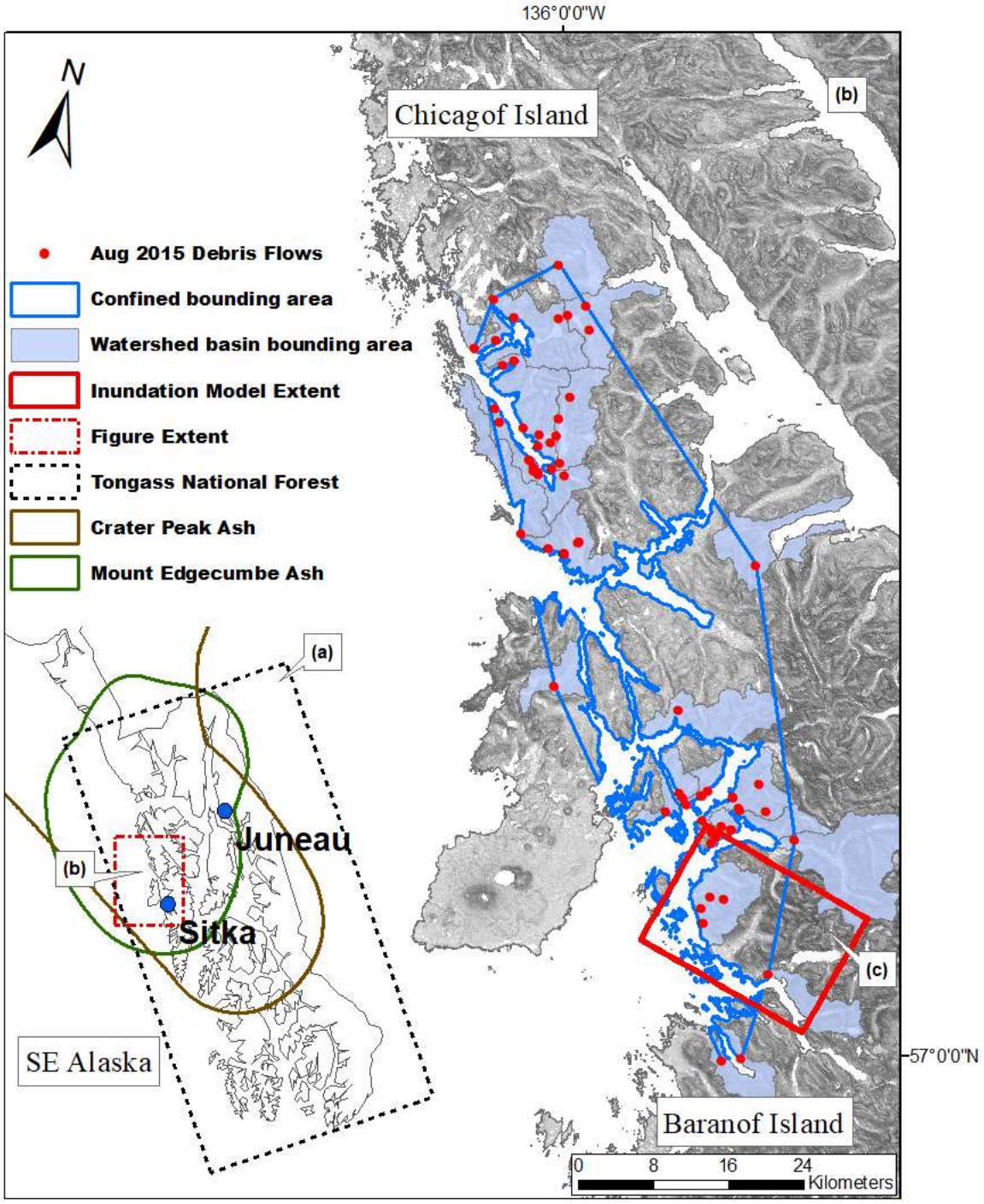

Figure 1. SE Alaska study areas corresponding to the three spatio-temporal scales analyzed in this study. (a) Inset map of SE Alaska, with the spatial extent of (b) indicated by the red dotted line and the extent of the Tongass National Forest (TNF) indicated by the dotted black line. Brown polyline represents extent of Tephra deposited by the 1992 Crater Peak eruption (Neal & others, 1995), green polyline represents extent of Mount Edgecombe Tephra deposits throughout the Holocene (Riehle & others, 1992). (b) Slope map of

study area with debris flows that occurred during a single storm event in August 2015 (red dots). Blue polygons represent an estimate of the "watershed basin" representative area impacted by landsliding delineated by HU-12 watershed boundaries from the National Hydrography Dataset. Blue outline represents an estimate of the "confined" representative area impacted by landsliding using a convex hull. (c) Solid red box represents the extent of the inundation model simulations.

2. Study area

The Tongass National Forest provides an ideal natural laboratory to study the amount and depositional fate of mobilized carbon through landsliding. The montane forests are mostly undisturbed by human activities, such as timber harvest, and are carbon dense, estimated to contain approximately 8% of all contiguous United States terrestrial biosphere carbon (Leighty et al., 2006). This region experiences large storms from the Pacific Ocean which trigger dozens to hundreds of landslides per event (Johnson et al., 2000). The lack of forest fires and insect infestations in the area allows us to isolate the effects of landslide disturbances on their potential to alter the regional carbon budget (Buma & Thompson, 2019).

2.1. Geology

Bedrock of the TNF study area near the Sitka focus area broadly consists of Late Cretaceous mudstones, as well as older volcaniclastic rock (Gehrels et al., 1994; Golder, 2001; Kramer et al., 2001). Pleistocene glacial activity has shaped the landscape of the region by carving the bedrock and forming U-shaped valleys, hanging valleys, and fjords (Golder, 2001; Hamilton and Thorsen, 1983; Hamilton, 1994; Kaufman and Manley, 2004). Much of the landscape is within close proximity to either fjords or the Pacific Ocean (Figure 1). West of Sitka rests Mount Edgecumbe, which has erupted basaltic to rhyolitic lava and ash dated to Paleogene and Quaternary periods (Gehrels et al., 1994).

Soils of the area are shallow and consist of weathered rhyolitic, dacitic, and andesitic ash sourced from Mount Edgecumbe (Riehl et al., 1992) underlain by glacial till. These ash beds can be as thick as 3 m in some locations near Sitka (Golder, 2001). Glacial deposits are prevalent throughout the region in the form of till, moraine, and outwash sediments and are positioned between volcanic ash and bedrock (Golder, 2001; Golder, 2008; Kramer et al., 2001). Both till and ash deposits have low permeability (Schroeder, 1983). Many landslides triggered near Sitka during the 2015 storm failed at the till-ash contact or within the till in the subsurface (Booth et al., 2020; Sitka Geotask Force, 2016). While the thicker ash beds are near Sitka, there are also regions in SE Alaska with high landslide densities, but little to no ash in the soils (Figure 1). Colluvial soils are present on lower slopes due to mass wasting events occurring after glacial retreat (Schroeder, 1983).

2.2. Southeast Alaska Climate

Southeast Alaska is classified as having a mid-latitude maritime climate with annual precipitation increasing with elevation, starting at 2.2 m yr^{-1} near sea level in Sitka (SNAP, 2018; Wendler et al., 2016). Average high temperatures are above freezing year-round (Shulski & Wendler, 2007). High winds and intense precipitation are common, often triggering debris flows within the region (Kramer et al., 2001; Yao et al., 2018). A storm on 18 August 2015 initiated over 60 landslides, many of which mobilized into debris flows (Fig. 1). Meteorological data (Horel et al., 2002) reported peak 3-hour rainfall intensity in Sitka at 33 mm hr^{-1}, a return period of 25-50 years, and a storm total of 140 mm rainfall in six hours at sea level (likely higher at elevation).

2.3. SE Alaska biomass and soil organic carbon estimations

Temperate rainforests have high carbon densities compared to other forests (Keith et al., 2009). Southeast Alaska contains an estimated 1.21 – 1.52 Pg C in aboveground biomass (Buma & Thompson, 2019) and 1.8 Pg SOC in an area of approximately 70,586 km^2 (McNicol et al., 2019). Parts of the region have been logged, but a majority of land contains old-growth forests (Berg et al., 2014). Previous estimations of C stocks within the TNF by Leighty et al. (2006) resulted in a total of 2.8 ± 0.5 Pg C for both biomass and soil (an average of 40,000 tC km^{-2}), an amount equating to 0.25% of the global terrestrial biosphere C. Carbon respiration in SE Alaska is relatively low compared to warmer, tropical climates (Raich & Schlesinger, 1992).

3. Methods

In this study, we combine landslide inventories with spatial models of soil and aboveground carbon to estimate mobilized carbon in SE Alaska for both a single storm event in 2015 and the historic record. We then estimate spatial patterns of debris flow runout over 10-ky time-scales with empirical runout modeling. Our methods generally follow West et al. (2011) and Hilton et al. (2011) by assessing carbon mobilization through landslide inventories and modeled carbon densities. We used the most comprehensive landslide inventory in SE Alaska, which was derived by historic aerial photo analysis and is maintained by the National Forest Service as the TNF Landslide Inventory (TongassLandslideAreas, 2018). In the following paragraphs, we detail the methods used for deriving mobilized carbon for the 2015 storm and historic record. We

then develop a 10-ky time-scale inundation model to determine the depositional fate of mobilized carbon.

3.1.1. Carbon models

Accurate modeling of carbon distributed throughout the SE Alaskan landscape is necessary for estimating mobilized carbon due to landsliding. We utilized two recent and comprehensive datasets which modeled C_{bio} and SOC across SE Alaska. Both datasets were developed using random decision forest algorithms to predict carbon density using environmental and disturbance variables coupled with Forestry Inventory and Analysis (FIA) data across the landscape (Buma & Thompson, 2019; McNicol et al., 2019). FIA plots are located approximately every 5 km throughout the United States, providing detailed data on forest conditions and the amount of aboveground biomass carbon at each plot (Barrett & Christensen, 2011). Random forest algorithms use classification and regression trees to determine significant variables in order to predict the amount of carbon stored in biomass and soil. The dominant variables that predicted C_{bio} were observed forest cover, slope, elevation, and likelihood of landslide initiation (Buma & Thompson, 2019) and for SOC the dominate variables were elevation, wetness, and slope position (McNicol et al., 2019). Biomass was converted to carbon at the standard rate of 50% (Houghton et al., 1996). The resulting products are C_{bio} and SOC continuous rasters for SE Alaska at resolutions of 30 m (C_{bio}) and 90.5 m (SOC) which we resampled using the nearest neighbor method to 5 m for consistency with an IfSAR-derived digital elevation model (DEM) to allow for finer resolution analysis with landslide polygons (US Geological Survey, 2017).

An observed vs. predicted fit r^2 value of 0.69 for biomass in FIA plots was reported by Buma and Thompson (2019) with carbon densities within landslide scars (mobilized C) containing a mean value of 36,557 ± 16,157 tC km^{-2} (mean ± standard deviation). The biomass models include a lower (58%) and upper (46%) carbon estimate which represent scaling factors to accommodate underestimation of aboveground biomass calculated in FIA forest plots as identified by Leighty et al. (2006). In this study, we compute mobilized C_{bio} for both the lower and upper biomass models and report the average, with the range as uncertainty. Average SOC estimated by McNicol et al. (2019) within landslide scars was 41,084 ± 9673 tC km^{-2} (mean ± standard deviation) with a predicted vs observed r^2 value of 0.73 and RMSE of 11,900 tC km^{-2}, indicating that, like the C_{bio} model, the SOC model reasonably predicts carbon across the landscape.

3.1.2. Mobilized carbon

For estimating mobilized carbon by the single storm, landslides in the TNF landslide inventory classified as occurring on 18 August 2015 labeled as debris torrent, debris avalanche, or combined debris avalanche and debris torrents were extracted. Longer term historic mobilization rates were completed by extracting all landslides in the TNF inventory similarly classified from the years 1960-2015. Although the TNF inventory includes landslides occurring before 1960, availability of remote imagery before 1960 is incomplete, and therefore we opted to not include those landslides. We computed two C mobilization rates within the TNF, with the minimum rate determined for the entire area covered by the TNF Landslide Inventory, and a maximum rate determined for a 7,431 km^2 area with the most complete mapping centered around Sitka.

The maximum rate is likely more representative of the true rate because it accounts for a likely observation bias in mapping more landslides near populated areas in the TNF landslide inventory. The C_{bio} and SOC rasters were clipped by the landslide polygons and summed to obtain the total C mobilized within the bounds of each landslide. Since debris flows typically mobilize all vegetation and soil down to bedrock within the initiation and runout zones, and disturb vegetation and soil via inundation in the depositional zone, we consider the entire polygons as being mobilized carbon.

3.2. Representative total area afflicted by landsliding

For debris flows triggered during the 2015 storm, a size of the event "footprint" is required for normalizing the rate of carbon mobilized by area, allowing comparison to other carbon mobilization studies. Two methods were used to delineate spatial extents of landsliding initiated (Figure 1). A "watershed basin" bounding area of 790 km^2 was defined as the total area of USGS National Hydrography 12-digit hydrologic units, which typically encompass 10,000-40,000 acres (USGS, 2018), that contained landslides. A "confined" bounding area of 1,103 km^2 was established via a convex hull of the point locations for the 2015 landslides. For both spatial extents, areas containing water (fjords, ocean, etc.) were excluded to only account for land affected by landsliding.

3.3. Long-term debris flow inundation modeling

Since analysis of the TNF Landslide Inventory offers a relatively short window of time compared to the timescales associated with carbon sequestration and respiration, we use empirical runout modeling to estimate the longer-term spatial pattern of debris flow deposition. An inundation model of a representative area with several U-shaped valleys

on northern Baranof Island (Figure 1) was developed to determine the depositional fate of mobilized carbon. We used the DFLOWZ inundation model, which is well-suited to simulating deposition of debris flows in confined channels and on unconfined hillslopes or fans (Berti & Simoni, 2007), with a previously developed landslide initiation susceptibility model for the region (Buma and Johnson, 2015) (Figure 2). The goal of these simulations was to produce a map of the long-term relative likelihood of debris flow deposition and estimate the average likelihood of deposits terminating in stream channels. Debris flows measured in the field to calibrate the model were mainly in undisturbed forests.

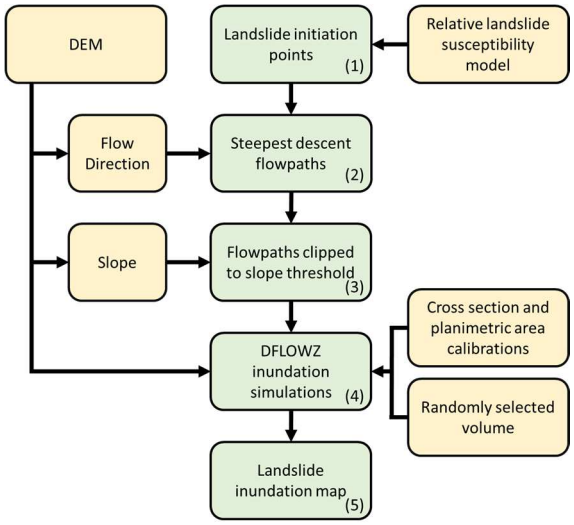

Figure 2. Flow chart describing steps taken (green boxes) and data needed (yellow boxes) for long-term inundation model. Numbers correspond to major steps shown in figure 3.

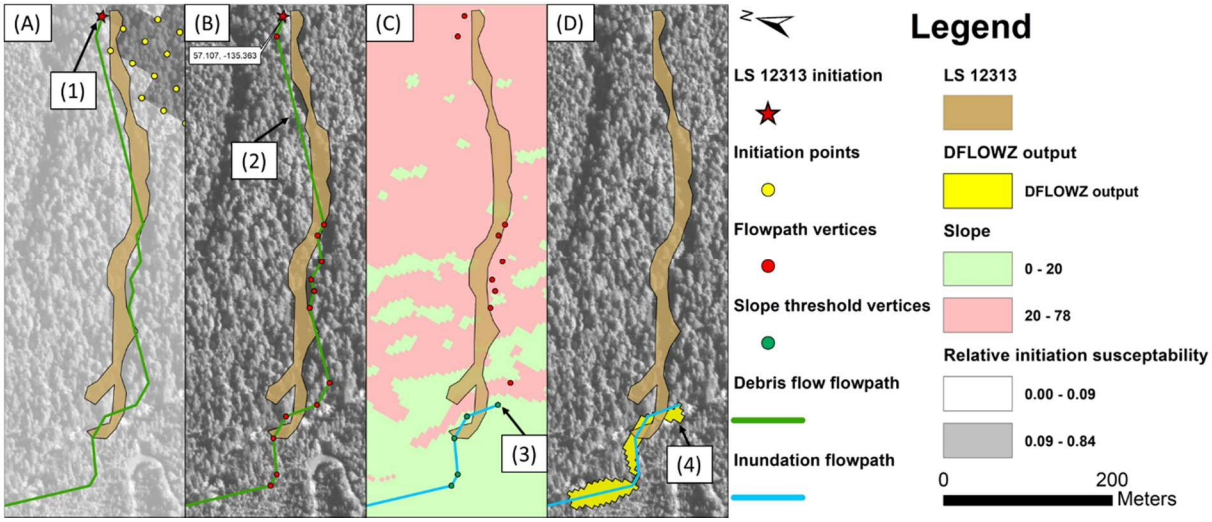

Figure 3. Example showing steps taken to model landslide inundation across northern Baranof Island. Numbers correspond to steps in flowchart (Figure 2). Brown polygon is a 2015 debris flow from the TNF inventory (LS #12313) near Sitka. (A) Background shading shows relative landslide initiation susceptibility raster with dark cells representing areas greater than the minimum initiation threshold for landslides that occurred during the 2015 storm and light cells representing areas that did not meet the threshold. Yellow points are locations that met the threshold and were processed for landslide inundation. Red star indicates the cell where landslide #12313 initiated, with a green polyline showing the debris flow steepest decent path. (B) Red points are flowpath polyline vertices of the steepest descent path. (C) Green points are polyline vertices below the 20° slope threshold for landslide deposition, and red points are above that threshold. Blue polyline reconstructed from vertices below 20° represents the flowpath for landslide deposition. (D) DFLOWZ output for the depicted flowpath using a field-measured volume of 6043 m^3. Aerial imagery-based inventories tend to underestimate runout length, which is reflected in the TNF polygon in this figure vs. our field observations.

3.3.1. Initiation points and volumes

For each simulated debris flow, DFLOWZ requires the location where deposition begins, the volume of the debris flow, a pathway which the debris flow would follow, and coefficients that quantify deposit geometry for calibrating depositional behavior. To establish where landslide initiation occurs, we used a relative landslide initiation susceptibility model for SE Alaska developed using a generalized linear model (Buma & Johnson, 2015). In that study, landslides mapped by the Tongass National Forest Service were analyzed for initiation site characteristics to produce a continuous model of relative initiation susceptibility at locations across the landscape. Significant variables used to model susceptibility were contributing area, slope, soil type, exposure to wind, and two

topographic indices. Four 2015 storm event landslides occurred within the inundation modeling study area (Figure 1), initiating in zones with relative susceptibility values ranging from 0.09 to 0.19. We therefore selected all pixels with relative susceptibility values greater than 0.09 as one set of locations for simulated landslide initiation (Figure 3 (A)). To capture the tendency for areas with higher relative susceptibilities to likely produce more landslides over time, we added a second set of initiation points that exceed a higher threshold of 0.19. In total, 28,089 points met the lower threshold, and an additional 8,171 points met the higher threshold, which were all processed for debris flow runout for a total of 36,260 simulations. Results for the inundation simulations represent approximately 32,000 years of landsliding on northern Baranof Island, assuming a background rate of 113 debris flows per century in the model domain (Barth et al., 2020). Each initiation point was assigned a random volume selected from a log-normal distribution of volumes (mean = 2830 m^3, sd = 6190 m^3) produced from field measurements near Sitka (Booth et al., 2020) (Appendix C).

3.3.2. Steepest descent flowpaths

A steepest descent flowpath from each initiation point was defined using the D8 flow direction algorithm (O'Callaghan & Mark, 1984) (Figure 3 (B)). The resulting flowpath represents the path by which a landslide would likely travel if initiated at the input point. A slope map derived from the 5m DEM was used to clip flowpaths to include only the depositional zone of a hypothetical debris flow from the respective initiation point. To do so, slope values were attached to vertex points from the steepest descent polylines. If a vertex slope value decreased below an approximate maximum depositional

threshold for SE Alaskan debris flows (20°) (Booth et al., 2020; Johnson et al., 2000), for more than 2 vertices in a row, the polyline above those vertices was removed. The resulting clipped polylines represent the flowpaths for debris flow deposition only and were subsequently fed into the DFLOWZ program to be processed for inundation prediction (Figure 3(C)).

3.3.3. DFLOWZ inundation simulations

Inundation is predicted through using semi-empirical relationships between debris flow volume, and the inundated cross-sectional and planimetric areas of a debris flow deposit. We refer to these relationships as "VAB equations" in this paper. Cross-sectional inundation area of the channel directly above the deposit is estimated by

$$A = aV^{2/3}, \quad (1)$$

where A is cross-sectional area inundated, V is debris flow volume, and a is a mobility coefficient. Similarly, planimetric area of the deposit is estimated by

$$B = bV^{2/3}, \quad (2)$$

where B is inundated planimetric area, and b is another mobility coefficient. The a and b mobility coefficients in equations (1) and (2) change according to debris flow characteristics such as grain-size, water content, and the presence of coarse woody debris (Crosta et al., 2003; Booth et al., 2020). When calibrated to fine-grained, large volume ($V > 10^7$ m^3) volcanic debris flows (lahars) Iverson et al. (1998) found $a = 0.05$ and $b = 200$ to be the best predictor of the total spatial inundation, based mainly on volcanic flank derived debris flows in the Pacific Northwest United States. Berti and Simoni (2007) derived VAB equations from published datasets of debris flows in the Italian Alps ($10^4 <$

$V < 10^9$ m^3) and found the coefficients $a = 0.08$ and $b = 17$ to be the best fit for unconfined debris flow deposits occurring mainly on fans. We use values of a = 0.11 and b = 8 for the mobility coefficients for this study, which have been calibrated for debris flows in SE Alaska (Booth et al., 2020). Detailed methods on debris flow field measurements are located in Appendix A.

3.4. Landslide inundation map

To map the spatial extent of deposition for each simulated debris flow with DFLOWZ, cross-sections were established every 40 m along the flow path (as defined in section 3.2.2) normal to the input flow direction polyline. These cross sections were then "filled" to a level such that the inundated cross-sectional area corresponded to the simulated debris flow volume according to eq. (1). Filling of the cross-sections proceeded down the flow path until the planform area of the deposit predicted by eq. (2) was reached (Figure 3 (D)). We repeated this process in a Monte Carlo approach for each polyline developed from each initiation point and each randomly selected volume (section 3.2.1). The final debris flow deposit inundation map is the sum of the number of times each cell in the DEM was inundated by a simulated debris flow (Figure 4a). A 50 m gaussian filter was then applied to more generally highlight areas of depositional "hotspots" from the resulting inundation simulations while smoothing the abrupt edges of the DFLOWZ results.

3.5. Stream connectivity

The depositional fate of mobilized carbon was determined via the depositional setting for both mapped and modeled debris flows. The inundation map developed in the

steps above allowed us to estimate the depositional fate of mobilized material transported by debris flows over millennial time scales, while actual inundated polygons from the TNF landslide inventory allowed us to determine historic stream connectivity. Stream deposition was defined as a landslide deposit intersecting the stream network from the National Hydrography Dataset (NHD) (USGS, 2018). A 10-meter buffer was applied to the stream network to account for possible lateral movement of streams within valleys as well as differences in mapping scale, resolution, and geospatial alignment of the DEM and NHD data sets (Figure 4 (B)). Stream widths in the region are not constant, therefore the 10 m buffer is a compromise between high and low order streams. The deposits that intersected the stream network were then separated from the total dataset to classify stream deposits (Figure 4 (C)). The most likely section of a debris flow to intersect with a stream is the debris flow snout, where woody debris tend to coalesce due to kinetic sieving (Iverson, 1997). Due to this, we consider any intersection between a debris flow and stream to be a 'stream deposit', but recognize that not all of the mobilized material ends up in the stream. For the TNF dataset, we defined connectivity as the total number of stream deposits divided by the total number of all deposits. Connectivity for the long-term runout model is defined as the number of times stream cells are inundated divided by the total number of times all cells are inundated.

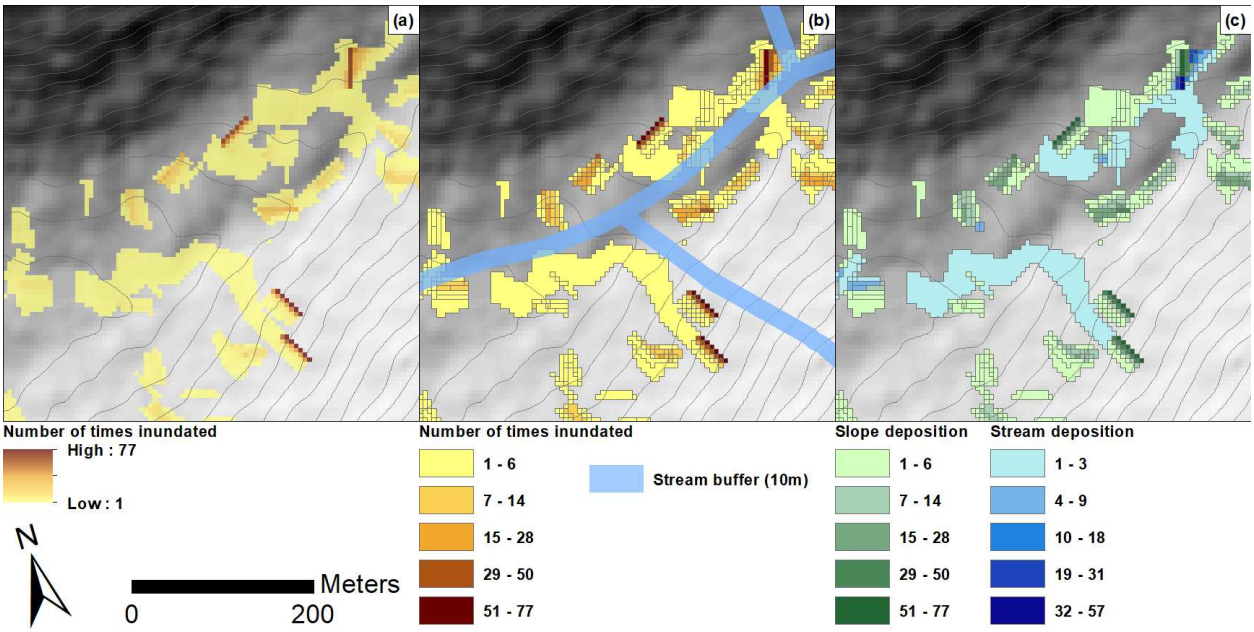

Figure 4. Example of (a) Inundation results with hillshade derived from 5m IfSAR DEM as background and 10 m contours. (b) Inundation results shown as individual landslide polygons with colors representing number of times each object was inundated, and the buffered stream network in blue. (c) Inundation results split between slope deposits (green color scale) and stream deposits (blue color scale). Location shown in Fig. 6.

4. Results

4.1. 2015 single storm event carbon mobilization

We estimate a total of 57,651 ± 3,266 tC was mobilized by 66 landslides with an area of 0.815 km^2 during the August 2015 storm, resulting in landslides mobilizing 70,672 ± 4,004 tC km^{-2} of landslide area. Using approximations of the "confined" area (1,103 km^2) and "watershed basin" area (790 km^2) affected by the storm (Figure 1) results in a range of 52 ± 3.0 to 73 ± 4.1 tC km^{-2} mobilized within the event "footprint" on Baranof and Chicagof Islands. Uncertainty is reported as the difference between the average of the 58% and 46% scaling C_{bio} models and the reported 11,900 tC km^{-2} RMSE for the SOC model added in quadrature (Appendix B).

The estimated values for mobilized carbon during the 2015 storm event provide us with a snapshot view of carbon mobilization during a single event in the SE Alaskan terrestrial biosphere. Taken into context, 57,651 ± 3,266 tC represents less than 0.01% of all carbon sequestered in SE Alaska. However, storm events that trigger debris flows are common in SE Alaska, allowing the opportunity for C mobilization to occur regularly in the TNF (Johnson et al., 2000). Using a return period of 25-50 years for storm frequency, we roughly estimate the C mobilization rate per year of a storm of this magnitude to be 2,306 ± 130 to 1,153 ± 65 tC yr^{-1} (Horel et al., 2002).

4.2. Century-scale carbon mobilization

Mobilized carbon via landsliding based on the TNF Landslide Inventory from 1960 to 2015 was 4.69 ± 0.21 MtC over the entirety of the TNF (70,586.56 km^2). This equates to 66.42 ± 2.9 tC km^{-2} with an annual rate of 1.21 ± 0.05 tC km^{-2} yr^{-1}. However, these values likely under-estimate the true rate of disturbance events for TNF, as landslide mapping efforts have been more concentrated near populated areas, such Sitka, AK (section 3.1.2). Using Baranof Island (area of 4,731 km^2) where Sitka is located, we compute a separate C mobilization rate with reduced observation bias that comes to a higher rate of 2.46 ± 0.12 tC km^{-2} yr^{-1} from landslide disturbance events. The 2015 storm represents approximately 1.2% of the total estimated carbon mobilized for the past 55 years within the TNF (4.69 ± 0.21 * 10^6 tC), which is about two-thirds of the annual C mobilized by landslides in an average year.

4.3. Spatial distribution of mobilized C in TNF

To visualize broad spatial patterns in C mobilization, a quartic kernel density function (Silverman, 1986), which smooths data points to calculate magnitude-per-area, was applied to the sum of SOC and C_{bio} distributions (tC km^{-2}), landslide occurrences km^{-2} (n = 7,156), and mobilized C_{bio} (tC km^{-2}) with a window size of 5 km and a cell size of 25 m. This highlights the broad distribution and magnitude of landslides and C throughout the landscape without being overly sensitive to specific, individual landslides (Figure 5). The spatial pattern of mobilized C density does not reflect the spatial pattern of landslide density or C density alone. Instead, the main driver for C mobilization across the region is moderate landslide densities occurring in high carbon areas. For example, the highest C mobilization densities tend to occur along the west coastline of the study area, where landslide density is moderate, and C is high (Fig. 5). Furthermore, the 70,672 ± 4,004 tC km^{-2} mobilized by landslides during the 2015 storm is higher than the landscape-wide average carbon density of 40,000 tC km^{-2} in the TNF (Leighty et al., 2006). In contrast, the regions with the highest landslide densities, for example >6 landslides per km^{-2} in the south-central part of the study area, correspond to moderate C mobilization, and regions with high C densities, but few landslides, have low C mobilization densities. Landslides primarily occurred on S-SW facing slopes, coinciding with regional wind patterns of S-SE aspects (Buma & Johnson, 2015; Harris, 1989), with an elevation of 337 ± 163 meters (mean ± sd).

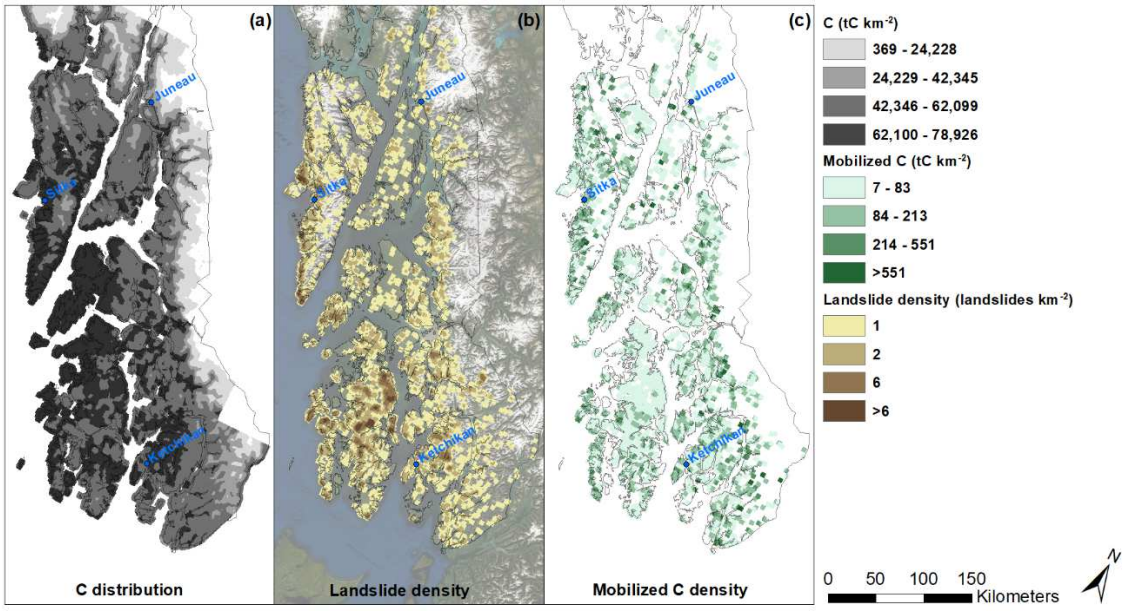

Figure 5. Spatial patterns of (a) summed SOC and C_{bio} (average between 46% and 58% adjusted C models from Buma and Thompson (2019)), (b) landslide density overlaying satellite imagery, and (c) mobilized C_{bio}, smoothed with a moving average quartic kernel with a window size of 5 km. Map extent of Fig. 1a.

4.3.1. Long-term depositional fate of mobilized C

Debris flow simulations across northern Baranof Island also indicate mobilized carbon 'hotspots' throughout the landscape (Figure 6). These hotspot locations experienced repeated inundation in the Monte Carlo simulations. Deposition hotspots are generally located on colluvial slopes below steep valley sidewalls in wide valleys, such as the Indian River valley, or in channels in the narrower valleys, such as Granite Creek and Cascade Creek. Some of the hotspot locations intersect with the road network for Sitka, indicating potential future hazards for Sitka residents and infrastructure (Figure 6). Valley geometry greatly influences whether landslides deposit into streams or not, with narrow valleys such as Granite Creek and Cascade Creek having a majority of the landslides connected to the stream network, and wide, U-shaped glacial valleys such as Indian River valley having few landslides connected to streams.

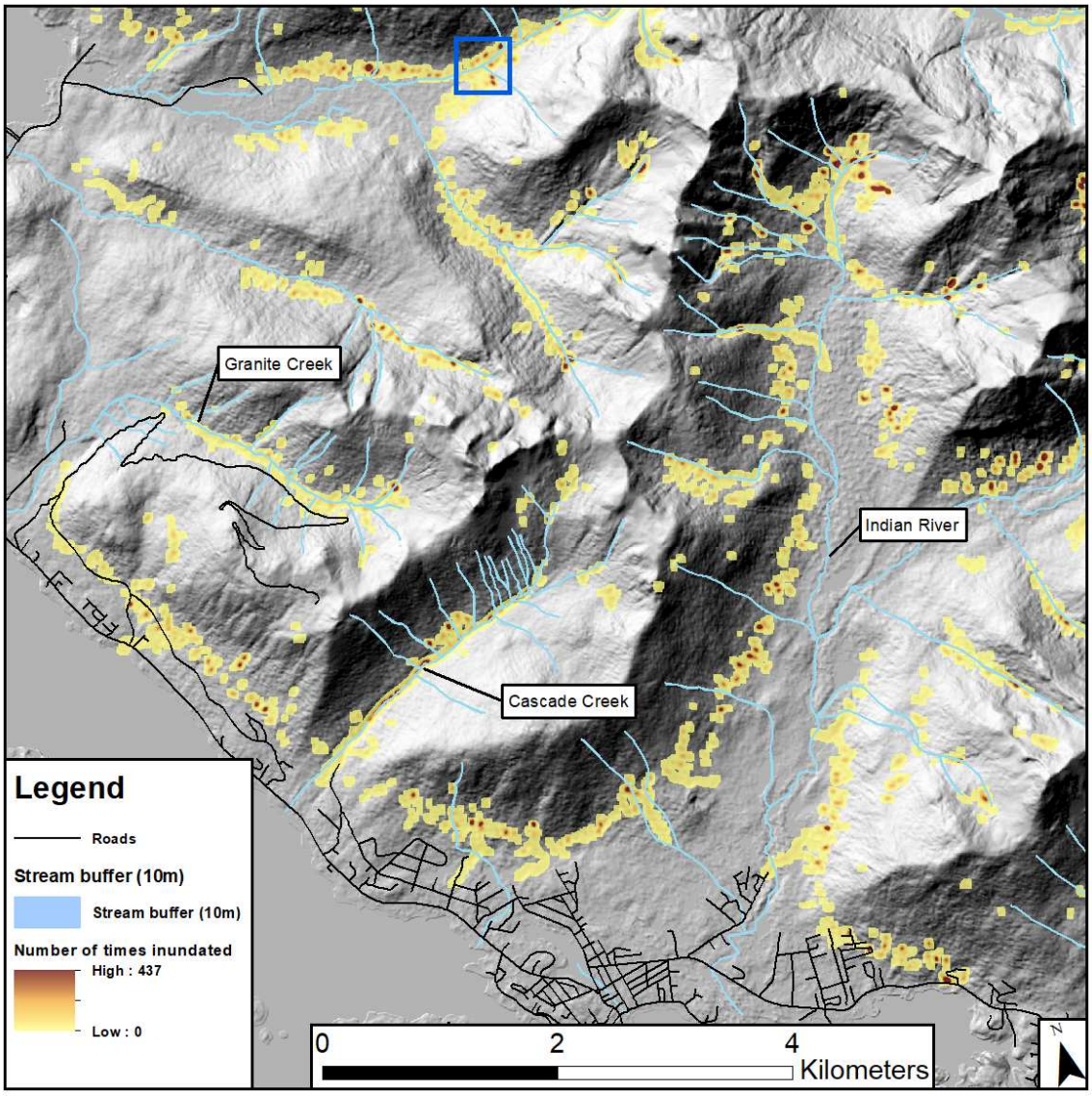

Figure 6. DFLOWZ simulation results smoothed by a 50 m gaussian filter overlaying a hillshade produced by a 5 m IFSAR DEM. Sitka road network indicated by black lines, and blue lines represent the USGS NHD flow lines, which represent streams with a 10 m buffer. The blue box indicates spatial extent for Figure 4, and the extent of the entire figure is shown in Fig. 1.

4.3.2. Connectivity analysis

Approximately 21% of the 66 debris flows triggered by the 2015 event were classified as stream deposits, with the remaining 79% of deposits classified as occurring

on hillslopes. An analysis of simulated debris flow inundation areas on northern Baranof Island resulted in 21.6% of the total inundated cells classified as stream deposits, with the remaining as hillslope deposition at 78.4%. These values are similar to the total TNF landslide connectivity rate which came to 24% stream deposits and 76% hillslope deposits. For the remainder of our analysis, we opt to use the TNF landslide connectivity rate, since it analyzes a larger area, and the magnitude is similar to the two other connectivity rates.

Landslide connectivity rates across the SE Alaskan landscape allows us to infer the likelihood of long-term sequestration of mobilized carbon. Due to streams meandering through floodplains, we consider these estimates to be a minimum. Of the 4.69 ± 0.21 MtC mobilized throughout the TNF over the 55-year period, 1.13 ± 0.05 MtC (24%) are estimated to have deposited to streams, where carbon can be metabolized, broken down into smaller particulate organic carbon (POC), or directly entrained by discharge and transported to water bodies for long-term sequestration. Residence times for POC in streams flowing through temperate forests in the Pacific Northwest have been estimated to be a few hundred years, indicating that although C metabolism does occur during stream transport, POC can be efficiently exported out of watersheds (Goñi et al., 2013). Conversely, the estimated C deposited on slopes equates to $3.56 \pm 0.16 * 10^6$ tC (76%), resulting in the burial of mobilized C into the soil horizons, leaching carbon and nutrients to the soil horizon (Hafner et al., 2005), or respirating CO_2 to the atmosphere.

5. Discussion

5.1. Estimated C mobilization rates and comparison

We used the best available data on landslides and C distribution to calculate C mobilization density and rates, but incompleteness of the landslide inventory likely caused an underestimation of those values. The TNF Landslide Inventory mapping effort, which is based on air photos and satellite imagery, is only as accurate as the available data. Specifically, historic landslides may be missed in the landslide inventory due to expeditious revegetation rates and low-resolution or incomplete historic aerial photography. The smallest mapped landslide within the inventory that mobilized C had an area of 40 m^2 and mobilized 2.2 tC. It would take 209,500 landslides of this size to change our estimate of mobilized C by 10%, suggesting that small landslides missing from the inventory do not substantially affect our overall results. Landslides that occur in low C density regions bring the mobilization rate down, reducing the representative rate of C mobilization occurring in forested areas throughout the TNF. Additional aerial LiDAR scanning and high-resolution air photos of the entirety of SE Alaska would greatly improve landslide mapping efforts as well as the understanding of revegetation rates for disturbed forests.

To place SE Alaskan C mobilization rates in a global context, we compiled studies that estimated C mobilization amount and rates for a variety of events that triggered landsliding around the world (Table 1). These studies are separated by event type (storm vs. earthquake), and sorted by latitude from the most northern to southern. It should be noted that many variables control C mobilization other than just the type of forest disturbance. Forest conditions vary between tropical and temperate forest types, and these may contribute to the varying C mobilization amounts and rates measured by these studies. With that in mind, there are few carbon mobilization studies to compare our

results to, and studies often do not report both single event mobilization amounts (tC km^{-2}) and long-term mobilization rates (tC km^{-2} yr^{-1}). The amount of C mobilized per event ranged from 13 to 680 tC km^{-2} over events with footprints ranging from 80 to 7500 km^2. Mobilization rates varied from 2.8 to 202 tC km^{-2} yr^{-1}. Events which mobilize the most C are earthquakes, however, long intervals between earthquakes result in lower annual rates (Table 1). Tropical storms mobilize moderate amounts of C, but occur on a more frequent basis relative to earthquakes and therefore tend to have higher C mobilization rates. Our estimated C mobilization amount for the 2015 storm event and the 55-year period mobilization rate within the TNF return comparable rates to previous work in the coastal Pacific Northwest (Madej, 2010), but relatively low C mobilization amount and rates in comparison to other, larger landslide mobilization events throughout the world (Table 1). One potential reason for relatively low C mobilization amount is our focus on landslides of only the debris flow class, in order to maintain consistency with inundation simulations using DFLOWZ. Landslides outside of the debris flow class are less frequent in SE Alaska, but do have the potential for mobilizing carbon. If included, our mobilization amount and rate would increase, potentially to a level that is comparable to other C mobilizing landslide events around the world. Rock, debris, and snow avalanches are one landslide type not included in this study, but they do occur in SE Alaska, and have the potential to mobilize carbon (Korup & Rixen, 2014).

Study	Location	Latitude	Disturbance event	tC km^{-2}	tC km^{-2} yr^{-1}	Carbon pool
This study[1]	SE Alaska	57° N	Single Storm	52.39 to 76.88	Varies	C_{bio}, BGC, SOC
This study[2]	SE Alaska	57° N	Multiple Storms	142.66 ± 7.7	2.59 ± 0.14	C_{bio}, BGC, SOC

Madej, 2010[3]	California	42° N	Storm	28	2.8	C_{bio}, SOC
Hilton & others, 2008	LiWu River, Taiwan	23° N	Tropical cyclone	13	16 to 202	C_{bio}, SOC
West & others, 2011[4]	Taiwan	23° N	Tropical cyclone	173.71	Varies	C_{bio}, BGC, SOC
Scharron & others, 2012	Guatemala	15° N	Hurricane	660	8 to 33	C_{bio}, SOC
Chen & others, 2009[5]	China	31° N	Earthquake	680	Varies	C_{bio}
Frith & others, 2018	Alpine fault, New Zealand	41° S	Earthquake	Varies	5 ± 2 to 9 ± 4	C_{bio}, SOC
Hilton & others, 2011	western Southern Alps, New Zealand	41° S	Earthquake	300 ± 110	7.6 ± 2.9	C_{bio}, SOC

Table 1. Compilation of disturbance related C mobilization events throughout the world. Notations: Aboveground Carbon (C_{bio}), Soil organic carbon (SOC), and Belowground Carbon (BGC) (root mass).

Note [1]2015 storm event estimated carbon mobilization amount. [2]Total mobilized C from biomass and SOC models over a 55-year period, normalized by Baranof Island area. [3]C mobilization normalized by watershed area. [4]Total biomass in trees, roots, soil litter mobilized during typhoon (12.5 Tg), normalized by area of Taiwan (35980 km^2), converted to Carbon at a rate of 50%. [5]Value computed based on Zhoa & Zhou (2006) forest density estimations and divided by the approximate area afflicted by the 2008 Wenchuan earthquake (20,000 km^2).

Another potential reason for our lower C mobilization amounts, when compared to earthquake events, is that precipitation-triggered debris flows tend to cover less area than earthquake-triggered landslides. Earthquakes can cause large swaths of hillslope area to fail due to seismic acceleration increasing driving stresses or weakening resisting forces of the slope (Newmark, 1965; Keefer, 1984). One such example is the M_w 7.9 Wenchuan earthquake that occurred in China, which triggered a total of >396 km^2 landslide area over an area of 20,000 km^2 (landslides were 2% of the earthquake affected area) during the single event, resulting in a 4-fold increase of POC export from river basins (Li et al., 2014). This earthquake triggered an estimated 600 tC km^{-2} during the event (Chen et al., 2009) (Table 1). In contrast, landslides triggered by the 2015 storm

near Sitka occupied <0.1% of the storm-affected area. Of Wenchuan earthquake-triggered landslides, approximately 16% were connected to streams, a value close to our estimated 20% in SE Alaska (Li et al., 2016). Similarly, an earthquake that occurred in central Taiwan was found to have 8% of earthquake triggered landslides connected to stream systems (Dadson et al., 2004). While earthquake triggered landslides tend to affect a larger proportion of the landscape than storm-triggered landslides in SE Alaska, C density in the TNF is higher than in the Wenchuan region of China and comparable to central Taiwan (McEwan et al., 2011; Qiu et al., 2015; Zhao & Zhou, 2006). However, the recurrence rate of storms initiating dozens of debris flows is higher relative to earthquakes, allowing the potential for carbon mobilization to occur more regularly in SE Alaska, which brings the relative rates between the two event-types closer together. Additionally, several active faults exist in SE Alaska which could have the potential for a mass initiation of landslides, however no data for earthquake triggered landslide events in the TNF currently exist (Doser et al., 1997). In a similar setting (Haida Gwaii, British Columbia), a magnitude 7.8 earthquake caused a 13-fold increase in annual landslide rate in the year of the earthquake (Barth et al., 2020). Last, an additional source for potential carbon sequestration via forest disturbances throughout SE Alaska could be a volcanic eruption from Mount Edgecombe. Previous eruptions coated the nearby landscape in ash, which served as a failure plane within soil profiles near Sitka (Sitka Geotask Force, 2016). In blanketing the forests with ash, SOC and organic litter is buried and potentially sequestered from the atmosphere, as has been observed in regions such as southern Chile (Mohr et al., 2017).

The period of time for carbon to recover after a landslide disturbance is difficult to ascertain, due to a lack of research in this area. Previous studies in SE Alaska found carbon accumulating at 300 tC km^{-2} yr^{-1} for C_{bio} in logged forests, reaching steady state density of 25,000 tC km^{-2} by around 500 years (Leighty et al., 2000). C accretion rates on landslides are likely slower due to the evacuation of soils, which require a period of time to re-develop and thus delay ecologic succession post-disturbance (Reneau & Dietrich, 1991; Reneau et al., 1990). Additionally, there are differences between secondary (some biomass still remains after disturbance) and primary (biomass completely gone) ecologic succession (Kimmins, 2004). Using the 300 tC km^{-2} yr^{-1} C_{bio} recovery for logged forests, it would take 110 years for mobilized C_{bio} to recover from the 2015 event. However, we make a conservative estimate of 120-150 years post disturbance to account for the delay in ecologic succession as a result of soil evacuation by landslides. SOC requires longer periods of time (on the order of milleniums) to recover relative to C_{bio} on the disturbed slopes due to the slow processes which accumulate organic material in soils (Kramer et al., 2004). Additionally, in filling of sediment on the margins of a debris flow track would likely expedite C recovery on a landslide scar. Windthrow disturbances in SE Alaskan watersheds were found to be drivers of SOC respiration by exhuming soil (Kramer et al., 2004). For landslide disturbances, organic soil stripped from slopes can be exposed at the surface in the deposit, where it can decompose and respire C to the atmosphere, but a greater portion of the mobilized soil is buried in the deposit relative to windthrow disturbances, resulting in short-term sequestration. Hillslope deposits can result in a net carbon sink or source depending on the rates of decomposition of

mobilized CWD and SOC, and the recovery of C on the disturbed slope, but further research is required to make this distinction.

For the remaining 24% of stream deposited material, we take into consideration Holocene carbon burial rates within fjords, dissolved organic carbon (DOC) stream levels, and total organic carbon in continental shelf sediment in the study region to assess the potential for those deposits to sequester C. Locally, SE Alaskan fjords are estimated to bury 0.265 tC km^{-2} yr^{-1}, where the area refers to watershed area draining to the fjord, a rate that is higher than other fjord systems in the world (Smith et al., 2015). In the context of our TNF landsliding rate of 2.46 ± 0.12 tC km^{-2} yr^{-1}, only 10% of the mobilized C would need to be exported to fjords to sustain this burial rate. It is reasonable to conclude that C mobilizing landslide events are contributing to the globally high rate of C burial in SE Alaskan fjords, but the precise proportion of POC transported from landslide deposits in streams to fjords is unknown. So, although C mobilization amount and rates in SE Alaska are generally low compared to areas with more extreme disturbances, the high connectivity of landslide deposits to the ocean and fjords via small mountain streams likely facilitates a high rate of carbon sequestration over geologic timescales.

Directly depositing material into fjord waters could also be a potential source for the higher C accumulation rates in SE Alaskan fjords. While few of the debris flows simulated with DFLOWZ deposited directly into fjords or to the Pacific Ocean due to a smaller area of interest being analyzed, field observations and mapped landslides indicated deposition frequently occurring directly into bodies of water. Based on aerial imagery of landslides initiated during the 2015 storm, 27% of the deposits occurred directly into or adjacent to a body of water, or a total of 45% of these landslides deposited

into either streams or bodies of water. The rate at which this occurs is likely higher in SE Alaska relative to other debris flow susceptible landscapes due to steep slopes adjacent to fjords and the Pacific Ocean. In regards to ocean delivered POC, continental shelves provide an opportunity for long-term storage of mobilized C that becomes buried. Sedimentation from fresh water discharge flowing from watersheds allows for transported POC to be buried in deltas on the SE Alaskan continental shelf, which is supported by the identification of land-derived C (1%-8% by weight) contained within coastal sediments (Walinsky et al., 2009). Landsliding allows additional sedimentation to occur on the coast, thus increasing the chance of POC to become buried if delivered to the continental shelf. Further research on the portion of CWD breaking down into POC and how much becomes buried in marine sediments would further constrain the magnitude of this geologic carbon sink.

An additional factor contributing to the C cycle is that deposition of C_{bio} and SOC in streams increases DOC as material decays over time. SE Alaskan stream samples measured by D'Amore et al. (2015) identified average area-weighted DOC flux to range from 10.5 to 29.9 tC km^{-2} yr^{-1} which correlated with hydropedologic units such as wetland soils. Although previous studies have identified lower DOC levels in streams that have been disturbed by logging (Hood, et al., 2006), it is likely that landslide disturbances, which transport rather than remove C from the landscape, contribute to the high stream DOC levels in SE Alaska, with an average of 18,700 ± 1,090 tC yr^{-1} being deposited into streams in the entire TNF. We infer the depositional fate of this landslide derived stream DOC to be transported downstream to bodies of water, where some mineralizes and becomes incorporated into lake sediments, but a majority respirates back

to the atmosphere (Algesten et al., 2005; Jansson et al., 2008; Vachon et al., 2017). We hypothesize that further research would reveal a correlation between stream DOC levels and deposited C by landsliding, similar to the post-POC increase in streams from the 2008 Wenchuan earthquake (Wang et al., 2016).

5.2. Simulated debris flow deposition and carbon mobilization "hotspots"

Our modeling results for debris flow deposition across the landscape of northern Baranof Island provide a unique opportunity to observe depositional "hotspots" for mobilized carbon that likely represent Holocene-scale patterns. Slopes or streams that are immediately downslope from steep topography typically are inundated by deposition multiple times, since multiple flow paths from different initiation sites tend to converge in such areas. The depositional start for the simulations at a slope threshold of 20° coincides with our field observations and previously measured landslide depositional slopes in the region (Booth et al., 2020; Johnson et al., 2000). It should be noted, however, that the initiation of landslide deposition is not solely dependent on a single slope threshold, but can be influenced by factors such as forest density and flow behavior (Fannin & Wise, 2001). Debris flows that recur at the same site before vegetation has had time to recover may therefore have different runout characteristics than debris flows occurring in undisturbed forest, which is assumed in our runout simulations.

Simulated deposits that intersect with the road network suggests areas potentially at risk, as some of these roads are adjacent to commercial or residential buildings. Furthermore, subtle changes to the topography due to landscaping for construction projects may not be reflected in the 5 m DEM used for delineating landslide flowpaths

for this project, which can cause inaccurate runout predictions in those areas. One such example of this is the fatal debris flow that occurred during the 2015 storm, in which the model interprets the steepest descent path from the DEM to be a path adjacent to a developing neighborhood, but the debris flow was impeded by dense forest and a subtle berm, potentially contributing to the debris flow routing into the neighborhood instead (Sitka Geotask Force, 2016).

Our study directly considered the relationship between landslide disturbances and C stocks within the TNF, and showed that moderate landslide disturbance in areas with dense C stocks resulted in the highest C mobilization rates. This differs from other forest disturbance events such as fires or insect infestations, which have the capacity to scale with available carbon. The results indicating C mobilization density is higher in regions that have higher C stocks coupled with moderate landslide density (Figure 5) support the ecological theory that higher C stocks correlate with moderate disturbances (Buma & Thompson, 2019; McLauchlan et al., 2014; Krannabetter et al., 2016). This is due to high disturbance regimes having frequent events which do not provide an opportunity for carbon to be reestablished, while low disturbance regimes experience biogeochemical limitations with the lack of nutrient recycling (Peltzer, et al., 2010). As carbon is transported from high on hillslopes to downslope sites where it is either buried or transported down streams, ecologic succession occurs on the disturbed slopes, contributing as a long-term carbon accreting mechanism. This process compounds over time as landslide-triggering storms allow for moderately disturbed areas to sequester large amounts of carbon at millennial timescales.

5.3. Implications for future carbon mobilization

Projected climate change rates for SE Alaska predict precipitation increasing by 6 to 18% in the next century (Shanley et al., 2015). This increase in annual precipitation is likely to trigger additional landslides (Crozier, 2010), either directly by making high intensity and duration rain storms more frequent or indirectly by broadly increasing antecedent soil moisture so that landslides are likely during less intense storms, thereby increasing the rate of debris flows occurring across the TNF. A direct result of increased landslide rates is the additional mobilization of SOC and C_{bio}, and the short to long term sequestration in soils and marine settings, providing a small buffer to increasing atmospheric CO_2 levels. Previous research for implications of climate change in SE Alaska primarily focuses on changes in net primary productivity (NPP), volumetric loss of glaciers, and impacts on fish habitats (Haufler, 2010; Shanley et al., 2015). A projected 20% increase in NPP for spruces is estimated for Alaska due to warming temperatures, but with this shift in climate comes an increase in respiration and decomposition processes (Keyser et al., 2000). With this projected increase in mind, a similar increase in landslide rates would be required to maintain the carbon accreting mechanism we have identified in this study.

6. Conclusions

We utilized landslide mapping and runout modeling in SE Alaska in conjunction with geospatial carbon density data of SOC and C_{bio} to estimate the amount of carbon mobilized by debris flows in SE Alaskan forests at two different spatio-temporal scales and predicted runout locations for a ~32,000-year timescale. A single storm in August 2015 mobilized 57,651 ± 3,266 tC, while debris flows across the entire TNF (70,586.56

km^2) mobilized 4.69 ± 0.21 MtC, a rate of 2.46 ± 0.12 tC km^{-2} yr^{-1} over the 55-year period analyzed. The annual rate is lower relative to other large-scale, landslide-mobilizing carbon events recorded in the world, such as tropical storms that impact SE Asia or earthquake triggered landslide events, primarily due to the higher landslide densities of those events. However, the geomorphic setting where landslides deposit can influence the depositional fate of mobilized carbon, affecting the temporal scale for C sequestration from the atmospheric pool. Using our modeled and actual landslide deposit locations in conjunction with the stream network across northern Baranof Island, we determined that approximately 21% of the landslides occurring in the region are ultimately connected to the modern stream network, while 24% are connected from analysis on the entire TNF landslide inventory. So, although the rate of C mobilization by debris flows in SE Alaska may be relatively low, much of that C may be efficiently transferred to marine basins, where it can become sequestered over geologic time scales. The depositional fate of stream and hillslope delivered C can only be inferred via our results, but landslides likely impact the regional carbon budget cycle. Furthermore, we found that C mobilization typically corresponds to moderate landslide frequency coupled with high C density, a result that may indicate SE Alaskan landslides contribute to the globally high carbon density of its forests. This work supports the emerging view that the link between landslide forest disturbances and erosion of organic carbon plays an important role in the global carbon cycle over geologic timescales.

References

Aleotti, P., & Chowdhury, R. (1999). Landslide hazard assessment: Summary review and new perspectives. Bulletin of Engineering Geology and the Environment, 58(1), 21–44.

Alexander, D. (2005). Vulnerability to landslides. Landslide Hazard and Risk, 175–198.

Algesten, G., Sobek, S., Bergström, A.-K., Jonsson, A., Tranvik, L. J., & Jansson, M. (2005). Contribution of sediment respiration to summer CO 2 emission from low productive boreal and subarctic lakes. Microbial Ecology, 50(4), 529–535.

Aller, R. C. (1998). Mobile deltaic and continental shelf muds as suboxic, fluidized bed reactors. Marine Chemistry, 61(3–4), 143–155.

Arriaga, F. J., & Lowery, B. (2005). Spatial distribution of carbon over an eroded landscape in southwest Wisconsin. Soil and Tillage Research, 81(2), 155–162.

Aumen, N. G., Bottomley, P. J., Ward, G. M., & Gregory, S. V. (1983). Microbial decomposition of wood in streams: Distribution of microflora and factors affecting [14C] lignocellulose mineralization. Appl. Environ. Microbiol., 46(6), 1409–1416.

Barrett, T. M., & Christensen, G. A. (2011). Forests of southeast and south-central Alaska, 2004–2008: Five-year forest inventory and analysis report. Gen. Tech. Rep. PNW-GTR-835. Portland, OR: US Department of Agriculture, Forest Service, Pacific Northwest Research Station. 156 p., 835.

Barth, S., Geertsema, M., Bevington, A. R., Bird, A. L., Clague, J. J., Millard, T., Bobrowsky, P. T., Hasler, A., & Liu, H. (2020). Landslide response to the 27 October 2012 earthquake (MW 7.8), southern Haida Gwaii, British Columbia, Canada. Landslides, 17(3), 517–526.

Berg, E. C., Gale, C. B., Morgan, T. A., Brackley, A. M., Keegan, C. E., Alexander, S. J., Christensen, G. A., McIver, C. P., & Scudder, M. G. (2014). Alaska's timber harvest and forest products industry, 2011. Gen. Tech. Rep. PNW GTR-903. Portland, OR: US Department of Agriculture, Forest Service, Pacific Northwest Research Station. 39 p., 903.

Berti, M., & Simoni, A. (2007). Prediction of debris flow inundation areas using empirical mobility relationships. Geomorphology, 90(1–2), 144–161. https://doi.org/10.1016/j.geomorph.2007.01.014

Booth, A. M., Sifford, C., Vascik, B., Siebert, C., & Buma, B. (2020). Large wood inhibits debris flow runout in forested southeast Alaska. Earth Surface Processes and Landforms. http://dx.doi.org/10.1002/esp.4830

Buma, B., & Johnson, A. C. (2015). The role of windstorm exposure and yellow cedar decline on landslide susceptibility in southeast Alaskan temperate rainforests. Geomorphology, 228, 504–511. https://doi.org/10.1016/j.geomorph.2014.10.014

Buma, B., & Thompson, T. (2019). Long-term exposure to more frequent disturbances increases baseline carbon in some ecosystems: Mapping and quantifying the disturbance frequency-ecosystem C relationship. PloS One, 14(2), e0212526.

Burdige, D. J. (2005). Burial of terrestrial organic matter in marine sediments: A re-assessment. Global Biogeochemical Cycles, 19(4).

Chambers, J. Q., Schimel, J. P., & Nobre, A. D. (2001). Respiration from coarse wood litter in central Amazon forests. Biogeochemistry, 52(2), 115–131.
Chen, H., Wu, N., Yuan, X., Gao, Y., & Zhu, D. (2009). Aftermath of the Wenchuan earthquake. Frontiers in Ecology and the Environment, 7(2), 72–72.
Chen, J. M., Ju, W., Cihlar, J., Price, D., Liu, J., Chen, W., Pan, J., Black, A., & Barr, A. (2003). Spatial distribution of carbon sources and sinks in Canada's forests. Tellus B: Chemical and Physical Meteorology, 55(2), 622–641.
Chen, X., Wei, X., & Scherer, R. (2005). Influence of wildfire and harvest on biomass, carbon pool, and decomposition of large woody debris in forested streams of southern interior British Columbia. Forest Ecology and Management, 208(1–3), 101–114.
Clark, K. E., West, A. J., Hilton, R. G., Asner, G. P., Quesada, C. A., Silman, M., Saatchi, S. S., Farfan-Rios, W., Martin, R. E., Horwath, A. B., & others. (2016). Storm-triggered landslides in the Peruvian Andes and implications for topography, carbon cycles, and biodiversity. Earth Surface Dynamics., 4(1), 47–70.
Crosta, G. B., Cucchiaro, S., & Frattini, P. (2003). Validation of semi-empirical relationships for the definition of debris-flow behavior in granular materials. Proceedings of the Third International Conference on Debris-Flow Hazards Mitigation: Mechanics, Prediction and Assessment, Davos, Switzerland. MillPress, Rotterdam, 821–831.
Crozier, M. J. (2010). Deciphering the effect of climate change on landslide activity: A review. Geomorphology, 124(3–4), 260–267. https://doi.org/10.1016/j.geomorph.2010.04.009
Cui, P., Hu, K., Zhuang, J., Yang, Y., & Zhang, J. (2011). Prediction of debris-flow danger area by combining hydrological and inundation simulation methods. Journal of Mountain Science, 8(1), 1–9.
Currie, W. S., Yanai, R. D., Piatek, K. B., Prescott, C. E., Goodale, C. L., & others. (2002). Processes affecting carbon storage in the forest floor and in downed woody debris. The Potential of US Forest Soils to Sequester Carbon and Mitigate the Greenhouse Effect, 135–157.
Dadson, S. J., Hovius, N., Chen, H., Dade, W. B., Lin, J.-C., Hsu, M.-L., Lin, C.-W., Horng, M.-J., Chen, T.-C., Milliman, J., & others. (2004). Earthquake-triggered increase in sediment delivery from an active mountain belt. Geology, 32(8), 733–736.
D'Amore, D. V., Edwards, R. T., Herendeen, P. A., Hood, E., & Fellman, J. B. (2015). Dissolved organic carbon fluxes from hydropedologic units in Alaskan coastal temperate rainforest watersheds. Soil Science Society of America Journal, 79(2), 378–388.
Dixon, R. K., & Turner, D. P. (1991). The global carbon cycle and climate change: Responses and feedbacks from below-ground systems. Environmental Pollution, 73(3), 245–262. https://doi.org/10.1016/0269-7491(91)90052-X
Doser, D. I., Pelton, J. R., & Veilleux, A. M. (1997). Earthquakes in the Pamplona zone, Yakutat block, south central Alaska. Journal of Geophysical Research: Solid Earth, 102(B11), 24499–24511.

Fan, S., Gloor, M., Mahlman, J., Pacala, S., Sarmiento, J., Takahashi, T., & Tans, P. (1992). A Large Terrestrial Carbon Sink in North America Implied by Atmospheric and Oceanic Carbon Dioxide Data and Models. Ecology., 73.

Fannin, R. J., & Wise, M. P. (2001). An empirical-statistical model for debris flow travel distance. Canadian Geotechnical Journal, 38(5), 982–994. https://doi.org/10.1139/cgj-38-5-982

Fiorillo, F., Guadagno, F., Aquino, S., & De Blasio, A. (2001). The December 1999 Cervinara landslides: Further debris flows in the pyroclastic deposits of Campania (southern Italy). Bulletin of Engineering Geology and the Environment, 60(3), 171–184.

Frith, N. V., Hilton, R. G., Howarth, J. D., Gröcke, D. R., Fitzsimons, S. J., Croissant, T., Wang, J., McClymont, E. L., Dahl, J., & Densmore, A. L. (2018). Carbon export from mountain forests enhanced by earthquake-triggered landslides over millennia. Nature Geoscience, 11(10), 772. https://doi.org/10.1038/s41561-018-0216-3

Froude, M. J., & Petley, D. N. (2018). Global fatal landslide occurrence from 2004 to 2016. Natural Hazards and Earth System Sciences, 18(8), 2161–2181.

Gehrels, G., Berg, H., & Plafker, G. (1994). Geology of southeastern Alaska. The Geology of Alaska.

Geotechnical Investigation Harbor Mountain road Sitka Alaska. (2001). Golder Associates Inc.

Geotechnical Report For Whitcomb Heights Stika (No. 073–95050; p. 19). (2008). Golder Associates Inc.

Goñi, M. A., Hatten, J. A., Wheatcroft, R. A., & Borgeld, J. C. (2013). Particulate organic matter export by two contrasting small mountainous rivers from the Pacific Northwest, USA. Journal of Geophysical Research: Biogeosciences, 118(1), 112–134.

Guzzetti, F., Reichenbach, P., Cardinali, M., Ardizzone, F., & Galli, M. (2003). The impact of landslides in the Umbria region, central Italy.

Hafner, S. D., Groffman, P. M., & Mitchell, M. J. (2005). Leaching of dissolved organic carbon, dissolved organic nitrogen, and other solutes from coarse woody debris and litter in a mixed forest in New York State. Biogeochemistry, 74(2), 257–282.

Hamilton, T. D. (1994). Late Cenozoic glaciation of Alaska. The Geology of Alaska, 1, 813–844.

Hamilton, T., & Thorson, R. (1983). The Cordilleran ice sheet in Alaska. Late Quaternary environments of the United States, Vol. 1, The late Pleistocene. University of Minnesota Press, Minneapolis, MN.

Harmon, M. E., Franklin, J. F., Swanson, F. J., Sollins, P., Gregory, S., Lattin, J., Anderson, N., Cline, S., Aumen, N. G., Sedell, J., & others. (1986). Ecology of coarse woody debris in temperate ecosystems. In Advances in ecological research (Vol. 15, pp. 133–302). Elsevier.

Haufler, J. (2010). Climate change: Anticipated effects on ecosystem services and potential actions by the Alaska Region, US Forest Service. DIANE Publishing.

Hilton, R. G. (2017). Climate regulates the erosional carbon export from the terrestrial biosphere. Geomorphology, 277, 118–132. https://doi.org/10.1016/j.geomorph.2016.03.028
Hilton, R. G., Galy, A., Hovius, N., Chen, M.-C., Horng, M.-J., & Chen, H. (2008). Tropical-cyclone-driven erosion of the terrestrial biosphere from mountains. Nature Geoscience, 1(11), 759–762. https://doi.org/10.1038/ngeo333
Hilton, R. G., Meunier, P., Hovius, N., Bellingham, P. J., & Galy, A. (2011). Landslide impact on organic carbon cycling in a temperate montane forest. Earth Surface Processes and Landforms, 36(12), 1670–1679. https://doi.org/10.1002/esp.2191
Hilton, R. G., & West, A. J. (2020). Mountains, erosion and the carbon cycle. Nature Reviews Earth & Environment, 1(6), 284–299.
Hood, E., Gooseff, M. N., & Johnson, S. L. (2006). Changes in the character of stream water dissolved organic carbon during flushing in three small watersheds, Oregon. Journal of Geophysical Research: Biogeosciences, 111(G1).
Horel, J., Splitt, M., Dunn, L., Pechmann, J., White, B., Ciliberti, C., Lazarus, S., Slemmer, J., Zaff, D., & Burks, J. (2002). Mesowest: Cooperative mesonets in the western United States. Bulletin of the American Meteorological Society, 83(2), 211–226.
Hotchkiss, E., Hall Jr, R., Sponseller, R., Butman, D., Klaminder, J., Laudon, H., Rosvall, M., & Karlsson, J. (2015). Sources of and processes controlling CO 2 emissions change with the size of streams and rivers. Nature Geoscience, 8(9), 696–699.
Houghton, J., Meira Filho, L., Lim, K., Trennton, I., Mamaty, I., Bonduki, Y., Griggs, D., & Callander, B. (1997). Revised 1996 IPCC Guidelines for National Greenhouse Gas Inventories, 1–3. Intergovernmental Panel on Climate Change. WMO/UNEP. Cambridge, UK: Cambridge University Press.
Iverson, R. M. (1997). The physics of debris flows. Reviews of Geophysics, 35(3), 245–296. https://doi.org/10.1029/97RG00426
Iverson, R. M., George, D. L., Allstadt, K., Reid, M. E., Collins, B. D., Vallance, J. W., Schilling, S. P., Godt, J. W., Cannon, C., Magirl, C. S., & others. (2015). Landslide mobility and hazards: Implications of the 2014 Oso disaster. Earth and Planetary Science Letters, 412, 197–208.
Iverson, R. M., Reid, M. E., & LaHusen, R. G. (1997). Debris-flow mobilization from landslides. Annual Review of Earth and Planetary Sciences, 25(1), 85–138.
Iverson, R. M., Schilling, S. P., & Vallance, J. W. (1998). Objective delineation of lahar-inundation hazard zones. Geological Society of America Bulletin, 110(8), 972–984.
Jaeger, J. M., Nittrouer, C. A., Scott, N. D., & Milliman, J. D. (1998). Sediment accumulation along a glacially impacted mountainous coastline: North-east Gulf of Alaska. Basin Research, 10(1), 155–173.
Jansson, M., Hickler, T., Jonsson, A., & Karlsson, J. (2008). Links between terrestrial primary production and bacterial production and respiration in lakes in a climate gradient in subarctic Sweden. Ecosystems, 11(3), 367–376.
Johnson, A. C., Swanston, D. N., & McGee, K. E. (2000). LANDSLIDE INITIATION, RUNOUT, AND DEPOSITION WITHIN CLEARCUTS AND OLD-GROWTH

FORESTS OF ALASKA. JAWRA Journal of the American Water Resources Association, 36(1), 17–30.
Kaufman, D. S., & Manley, W. F. (2004). Pleistocene maximum and Late Wisconsinan glacier extents across Alaska, USA. In Developments in Quaternary Sciences (Vol. 2, pp. 9–27). Elsevier.
Keefer, D. K. (1984). Landslides caused by earthquakes. Geological Society of America Bulletin, 95(4), 406–421.
Keith, H., Mackey, B. G., & Lindenmayer, D. B. (2009). Re-evaluation of forest biomass carbon stocks and lessons from the world's most carbon-dense forests. Proceedings of the National Academy of Sciences, 106(28), 11635–11640.
Keyser, A. R., Kimball, J. S., Nemani, R. R., & Running, S. W. (2000). Simulating the effects of climate change on the carbon balance of North American high-latitude forests. Global Change Biology, 6(S1), 185–195.
Kimmins, J. P. (2004). Forest ecology. Fishes and Forestry: Worldwide Watershed Interactions and Management, 17–43.
Korup, O., & Rixen, C. (2014). Soil erosion and organic carbon export by wet snow avalanches. The Cryosphere, 8(2), 651–658.
Kramer, M. G., Hansen, A. J., Taper, M. L., & Kissinger, E. J. (2001). Abiotic Controls on Long-Term Windthrow Disturbance and Temperate Rain Forest Dynamics in Southeast Alaska. Ecology, 82(10), 2749–2768. https://doi.org/10.1890/0012-9658(2001)082[2749:ACOLTW]2.0.CO;2
Kramer, M. G., Sollins, P., & Sletten, R. S. (2004). Soil carbon dynamics across a windthrow disturbance sequence in southeast Alaska. Ecology, 85(8), 2230–2244.
Kranabetter, J. M., McLauchlan, K. K., Enders, S. K., Fraterrigo, J. M., Higuera, P. E., Morris, J. L., Rastetter, E. B., Barnes, R., Buma, B., Gavin, D. G., & others. (2016). A framework to assess biogeochemical response to ecosystem disturbance using nutrient partitioning ratios. Ecosystems, 19(3), 387–395.
Lancaster, S. T., Hayes, S. K., & Grant, G. E. (2003). Effects of wood on debris flow runout in small mountain watersheds: EFFECTS OF WOOD ON DEBRIS FLOW RUNOUT. Water Resources Research, 39(6). https://doi.org/10.1029/2001WR001227
Leighty, W. W., Hamburg, S. P., & Caouette, J. (2006). Effects of Management on Carbon Sequestration in Forest Biomass in Southeast Alaska. Ecosystems, 9(7), 1051–1065. https://doi.org/10.1007/s10021-005-0028-3
Li, G., West, A. J., Densmore, A. L., Hammond, D. E., Jin, Z., Zhang, F., Wang, J., & Hilton, R. G. (2016). Connectivity of earthquake-triggered landslides with the fluvial network: Implications for landslide sediment transport after the 2008 Wenchuan earthquake. Journal of Geophysical Research: Earth Surface, 121(4), 703–724.
Li, G., West, A. J., Densmore, A. L., Jin, Z., Parker, R. N., & Hilton, R. G. (2014). Seismic mountain building: Landslides associated with the 2008 Wenchuan earthquake in the context of a generalized model for earthquake volume balance. Geochemistry, Geophysics, Geosystems, 15(4), 833–844.
Madej, M. A. (2010). Redwoods, restoration, and implications for carbon budgets. Geomorphology, 116(3–4), 264–273.

Marra, J. L., & Edmonds, R. L. (1994). Coarse woody debris and forest floor respiration in an old-growth coniferous forest on the Olympic Peninsula, Washington, USA. Canadian Journal of Forest Research, 24(9), 1811–1817.
May, C. L. (2002). Debris flows through different forest age classes in the Central Oregon Coast Range. JAWRA Journal of the American Water Resources Association, 38(4), 1097–1113.
McEwan, R. W., Lin, Y.-C., Sun, I.-F., Hsieh, C.-F., Su, S.-H., Chang, L.-W., Song, G.-Z. M., Wang, H.-H., Hwong, J.-L., Lin, K.-C., & others. (2011). Topographic and biotic regulation of aboveground carbon storage in subtropical broad-leaved forests of Taiwan. Forest Ecology and Management, 262(9), 1817–1825.
McLauchlan, K. K., Higuera, P. E., Gavin, D. G., Perakis, S. S., Mack, M. C., Alexander, H., Battles, J., Biondi, F., Buma, B., Colombaroli, D., & others. (2014). Reconstructing disturbances and their biogeochemical consequences over multiple timescales. BioScience, 64(2), 105–116.
McNicol, G., Bulmer, C., D'Amore, D., Sanborn, P., Saunders, S., Giesbrecht, I., Arriola, S. G., Bidlack, A., Butman, D., & Buma, B. (2019). Large, climate-sensitive soil carbon stocks mapped with pedology-informed machine learning in the North Pacific coastal temperate rainforest. Environmental Research Letters, 14(1), 014004.
Medeiros, A., Pascoal, C., & Graça, M. (2009). Diversity and activity of aquatic fungi under low oxygen conditions. Freshwater Biology, 54(1), 142–149.
Milliman, J. D., & Syvitski, J. P. (1992). Geomorphic/tectonic control of sediment discharge to the ocean: The importance of small mountainous rivers. The Journal of Geology, 100(5), 525–544.
Mohr, C. H., Korup, O., Ulloa, H., & Iroumé, A. (2017). Pyroclastic eruption boosts organic carbon fluxes into Patagonian fjords. Global Biogeochemical Cycles, 31(11), 1626–1638.
Newmark, N. M. (1965). Effects of earthquakes on dams and embankments. Geotechnique, 15(2), 139–160.
Peltzer, D. A., Wardle, D. A., Allison, V. J., Baisden, W. T., Bardgett, R. D., Chadwick, O. A., Condron, L. M., Parfitt, R. L., Porder, S., Richardson, S. J., & others. (2010). Understanding ecosystem retrogression. Ecological Monographs, 80(4), 509–529.
Progar, R., Schowalter, T., Freitag, C., & Morrell, J. J. (2000). Respiration from coarse woody debris as affected by moisture and saprotroph functional diversity in Western Oregon. Oecologia, 124(3), 426–431.
Qiu, S., Xu, M., Zheng, Y., Li, R., Wong, M. H. G., Zhang, L., Liu, L., Lai, C., & Zhang, W. (2015). Impacts of the Wenchuan earthquake on tree mortality and biomass carbon stock. Natural Hazards, 77(2), 1261–1274.
Ramos Scharrón, C. E., Castellanos, E. J., & Restrepo, C. (2012). The transfer of modern organic carbon by landslide activity in tropical montane ecosystems. Journal of Geophysical Research: Biogeosciences, 117(G3). https://doi.org/10.1029/2011JG001838
Reid, M. E., Coe, J. A., & Brien, D. L. (2016). Forecasting inundation from debris flows that grow volumetrically during travel, with application to the Oregon Coast

Range, USA. Geomorphology, 273, 396–411. https://doi.org/10.1016/j.geomorph.2016.07.039
Reneau, S. L., & Dietrich, W. E. (1991). Erosion rates in the southern Oregon Coast Range: Evidence for an equilibrium between hillslope erosion and sediment yield. Earth Surface Processes and Landforms, 16(4), 307–322.
Reneau, S. L., Dietrich, W. E., Donahue, D. J., Jull, A. T., & Rubin, M. (1990). Late Quaternary history of colluvial deposition and erosion in hollows, central California Coast Ranges. Geological Society of America Bulletin, 102(7), 969–982.
Restrepo, C., Vitousek, P., & Neville, P. (2003). Landslides significantly alter land cover and the distribution of biomass: An example from the Ninole ridges of Hawai'i. Plant Ecology, 166(1), 131–143.
Rickenmann, D. (1999). Empirical relationships for debris flows. Natural Hazards, 19(1), 47–77.
Riehle, J. R., Champion, D. E., Brew, D. A., & Lanphere, M. A. (1992). Pyroclastic deposits of the Mount Edgecumbe volcanic field, southeast Alaska: Eruptions of a stratified magma chamber. Journal of Volcanology and Geothermal Research, 53(1–4), 117–143.
Rumpel, C., Kögel-Knabner, I., & Bruhn, F. (2002). Vertical distribution, age, and chemical composition of organic carbon in two forest soils of different pedogenesis. Organic Geochemistry, 33(10), 1131–1142.
Russell, M. B., Fraver, S., Aakala, T., Gove, J. H., Woodall, C. W., D'Amato, A. W., & Ducey, M. J. (2015). Quantifying carbon stores and decomposition in dead wood: A review. Forest Ecology and Management, 350, 107–128. https://doi.org/10.1016/j.foreco.2015.04.033
Scheidl, C., & Rickenmann, D. (2010). Empirical prediction of debris-flow mobility and deposition on fans. Earth Surface Processes and Landforms, 35(2), 157–173. https://doi.org/10.1002/esp.1897
Schilling, S. P. (1998). LAHARZ; GIS programs for automated mapping of lahar-inundation hazard zones. US Geological Survey; Information Services [distributor],.
Schimel, D. S., Braswell, B., Holland, E. A., McKeown, R., Ojima, D. S., Painter, T. H., Parton, W. J., & Townsend, A. R. (1994). Climatic, edaphic, and biotic controls over storage and turnover of carbon in soils. Global Biogeochemical Cycles, 8(3), 279–293.
Schroeder, W. L. (1983). Geotechnical Properties of Southeast Alaskan Forest Soils (pp. 1–46). Oregon State University.
Shanley, C. S., Pyare, S., Goldstein, M. I., Alaback, P. B., Albert, D. M., Beier, C. M., Brinkman, T. J., Edwards, R. T., Hood, E., MacKinnon, A., & others. (2015). Climate change implications in the northern coastal temperate rainforest of North America. Climatic Change, 130(2), 155–170.
Shulski, M., & Wendler, G. (2007). The climate of Alaska. University of Alaska Press.
Silverman, B. W. (1986). Density estimation for statistics and data analysis (Vol. 26). CRC press.

Sitka Geotask Force Summaries August 2015 Sitka Landslides. (2016). Sitka Sound Science Center.
Smith, R. W., Bianchi, T. S., Allison, M., Savage, C., & Galy, V. (2015). High rates of organic carbon burial in fjord sediments globally. Nature Geoscience, 8(6), 450.
SNAP. (2018). Scenarios Network for Alaska and Arctic Planning: Historical Monthly Temperature and Precipitation and Historical Derived Temperature Products.
Stallard, R. F. (1998). Terrestrial sedimentation and the carbon cycle: Coupling weathering and erosion to carbon burial. Global Biogeochemical Cycles, 12(2), 231–257. https://doi.org/10.1029/98GB00741
Stock, J. D., & Dietrich, W. E. (2006). Erosion of steepland valleys by debris flows. Geological Society of America Bulletin, 118(9–10), 1125–1148.
Tongass National Forest, USDA Forest Service, R10, Tongass National Forest. (20190813). TongassLandslidesAreas.
Triska, F. J., & Cromack Jr, K. (1980). The role of wood debris in forests and streams. Forests: Fresh Perspectives from Ecosystem Analysis. Oregon State University Press, Corvallis, Oregon, USA, 171–190.
Turowski, J. M., Hilton, R. G., & Sparkes, R. (2016). Decadal carbon discharge by a mountain stream is dominated by coarse organic matter. Geology, 44(1), 27–30.
U.S. Geological Survey. (2017). 5 Meter Alaska Digital Elevation Mdoels (DEMs)—USGS National Map 3DEP. Downloadable Data Collection: U.S. Geological Survey.
U.S. Geological Survey, National Geospatial Program. (2018). USGS National Hydrography Dataset (NHD) Best Resolution HU8-9 20180304 for HU-8 Subbasin FileGDB 10.1 Model Version 2.2.1.
Vachon, D., Prairie, Y. T., Guillemette, F., & Del Giorgio, P. A. (2017). Modeling allochthonous dissolved organic carbon mineralization under variable hydrologic regimes in boreal lakes. Ecosystems, 20(4), 781–795.
Walinsky, S., Prahl, F., Mix, A., Finney, B., Jaeger, J., & Rosen, G. (2009). Distribution and composition of organic matter in surface sediments of coastal Southeast Alaska. Continental Shelf Research, 29(13), 1565–1579.
Wang, J., Jin, Z., Hilton, R. G., Zhang, F., Li, G., Densmore, A. L., Gröcke, D. R., Xu, X., & West, A. J. (2016). Earthquake-triggered increase in biospheric carbon export from a mountain belt. Geology, 44(6), 471–474.
Wang, Y., Law, R., & Pak, B. (2010). A global model of carbon, nitrogen and phosphorus cycles for the terrestrial biosphere. Biogeosciences, 7(7), 2261–2282.
Wendler, G., Galloway, K., & Stuefer, M. (2016). On the climate and climate change of Sitka, Southeast Alaska. Theoretical and Applied Climatology, 126(1–2), 27–34.
West, A. J., Lin, C.-W., Lin, T.-C., Hilton, R. G., Liu, S.-H., Chang, C.-T., Lin, K.-C., Galy, A., Sparkes, R. B., & Hovius, N. (2011). Mobilization and transport of coarse woody debris to the oceans triggered by an extreme tropical storm. Limnology and Oceanography, 56(1), 77–85. https://doi.org/10.4319/lo.2011.56.1.0077
Wiebe, S. A., Morris, D. M., Luckai, N. J., & Reid, D. E. (2014). The influence of coarse woody debris on soil carbon and nutrient pools 15 years after clearcut harvesting

in black spruce—Dominated stands in northwestern Ontario, Canada. Écoscience, 21(1), 11–20.
Yao, Y., Zhong, Z., Yang, X.-Q., & Huang, X. (2018). Seasonal variation of the North Pacific storm-track relationship with the Subarctic frontal zone intensity. Dynamics of Atmospheres and Oceans, 83, 75–82. https://doi.org/10.1016/j.dynatmoce.2018.06.003
Zhao, M., & Zhou, G.-S. (2006). Carbon storage of forest vegetation in China and its relationship with climatic factors. Climatic Change, 74(1–3), 175–189.

Appendix

Appendix A. Field measurements

Of the 66 debris flows from the 2015 event, 19 debris flows were visited in the field over two field seasons and were measured for deposit volume, maximum inundated cross-section area, deposit slope, and planimetric area. Deposit volumes were estimated via measuring the widths and depths, where possible, of deposits in segments. If obtaining deposit depth proved to be difficult, the slope of the channel above and below the deposit was measured with an inclinometer and then the channel slope directly below the deposit was interpolated. Profile measurements taken on the deposit were then used with the interpolated channel slope to estimate depths if direct measurements were not possible. Measured segments had volumes computed via geometric equations and then summed to obtain deposit volumes. A second method used was assuming ellipsoidal geometry of deposits and estimating volume via the equations

$$V = \frac{4}{3}\pi * ABC \tag{3}$$

for an ellipsoid and

$$V = \frac{2}{3}\pi * ABC \tag{4}$$

for a half-ellipsoid, where A, B, and C are the three perpendicular axes of ellipsoidal objects. At each debris flow, an average cross-sectional area was computed from three measured cross-sections using measuring tapes. Depositional slope was measured using an inclinometer adjacent to the debris flow deposit on hillslopes or within the stream channel where possible. Planimetric area for deposits was acquired via the summed geometric sections used for estimating volume. Field measurements were used to plot

VAB relationships for SE Alaska debris flow runout characteristics used to calibrate DFLOWZ for runout simulations (section 3.3.3) (Figure 7).

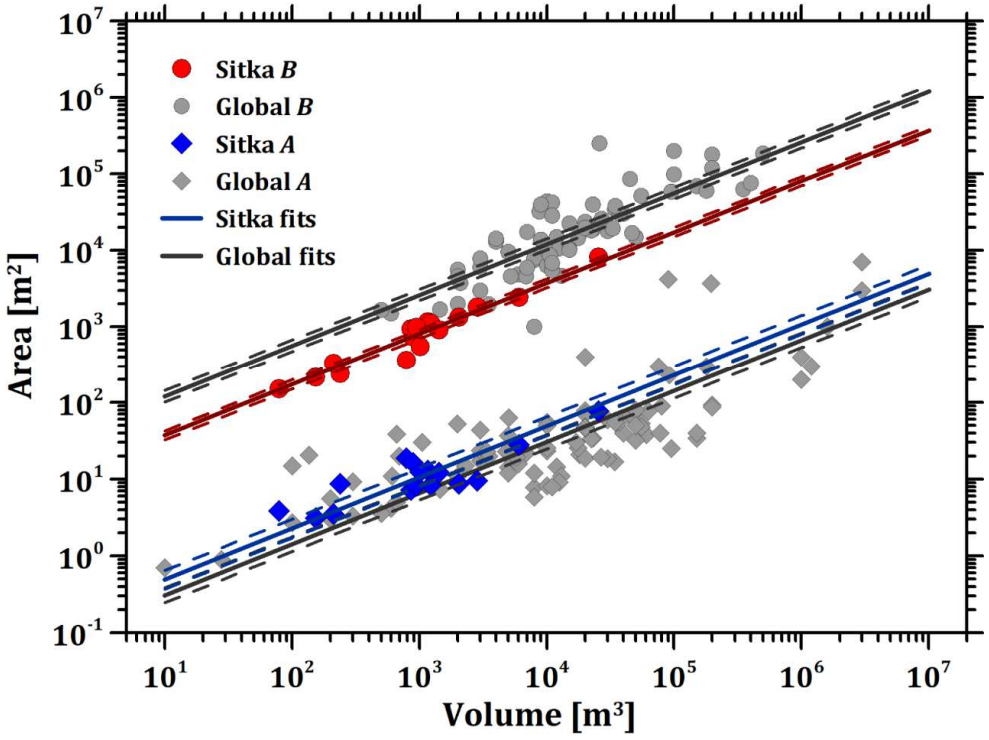

Figure 7. Volume-planimetric area (B) and volume-cross sectional area (A) results for debris flows measured near Sitka (Booth et al., 2020). Background points are sourced from areas outside of SE Alaska as a comparison to other debris flow runout characteristics (Berti & Simoni, 2007; Griswold & Iverson, 2008; Webb et al., 2008; D'Agostino et al., 2010; Scheidl & Rickenmann, 2010; Simoni et al., 2011).

ID number†	UTM Easting [m]	UTM Northing [m]	*V* [m³]	*A* [m²]	*B* [m²]	*H* [m]	*L* [m]	*L/H*	Deposit slope [°]
12312	477,165	6,327,810	25,390	77.2	8,281	405	698	1.7	15.5
12313	477,784	6,329,166	6,043	27.9	2,455	228	527	2.3	6
12336	474,943	6,340,035	79	3.9	152	61	93	1.5	15.7
12338	474,325	6,339,480	1,156	13	1,167	165	222	1.3	24
12341	471,986	6,339,097	153	3.1	216	76	189	2.5	9
12343	470,999	6,336,895	789	18.8	367	105	327	3.1	8.5
12349	477,687	6,340,096	892	16.4	741	57	107	1.9	11.6
12350	477,720	6,340,025	1,221	8.3	1,112	58	112	1.9	14.5
12356	476,545	6,334,728	2,830	9.6	1,832	149	450	3	9.7
12358	476,891	6,335,406	858	7.3	940	81	99	1.2	25.5
12413	483,096	6,312,493	211	3.5	332	51	121	2.4	11.6
12415	485,094	6,313,280	945	8.4	990	484	730	1.5	16.5
12339	472,995	6,338,098	238	9	240	63	100	1.6	16
12314	485,771	6,322,635	1,567	7	510	53	103	1.9	0
12646	479,854	6,335,217	1,418	12	915	56	152	2.7	11
no ID	472,130	6,337,685	479	8	400	69	160	2.3	12
12437	478,920	6,325,213	2,036	9	1,352	467	816	1.7	16
17145	482,477	6,328,162	1,010	12	554	263	500	1.9	9
12311	477,705	6,326,307	10,043		27,694	392	824	2.1	13

Table 2. Measured landslides from field work. Separation line above ID number 12339 designates 2018 and 2019 field seasons. Columns are UTM Easting and Northing coordinates, deposit volume (*V*), cross-sectional area (*A*), planimetric area (*B*), height of landslide from initiation point to deposition elevations (*H*), length of landslide runout (*L*), the length to height ratio (*L/H*), and the slope of the deposit. Landslide ID number 12311 volume is red due to a separate method of acquiring volume, which was through the number of dump trucks that removed debris from a developing neighborhood where the landslide deposited. This value has an error margin that is hard to predict relative to the other volumetric estimation method.

Appendix B. Measured mobilized C

Supplemental file 'MeasuredLandslideCarbon.csv' (file size 336 KB, requires Microsoft Excel) includes every landslide meeting the debris flow criteria (section 3.1.2) are listed with their TNF landslide inventory ID (column TNF_LS_NO). Included for each landslide are whether the landslide is located on Baranof Island, whether the landslide was initiated during the 2015 event, the size of the landslide in ha and km^2, and the three mobilized carbon amounts from the 46% and 58% scaled C_{bio} models and SOC model. The amounts shown are computed using the methods detailed in section 3.1.2, summarized by the equation

$$tC = \frac{tC}{ha} * ha \tag{5}$$

where *tC* = tonnes of carbon, and *ha* = area of the landslide in hectares. Errors for mobilized C were computed in the following equations

$$C_{bio}err = \frac{{C_{bio}}^{46\%} + {C_{bio}}^{58\%}}{2} \tag{6}$$

$$SOCerr = 119 * \sqrt{N} \tag{7}$$

$$total\ error = \sqrt{C_{bio}err^2 + SOCerr^2} \tag{8}$$

where N = number of pixels from the SOC model clipped by landslides, ${C_{bio}}^{46\%}$ and ${C_{bio}}^{58\%}$ represent the two scaled C_{bio} models, and *total error* is the two errors added in quadrature.

Appendix C. Debris flow runout model description and volume distribution

The debris flow runout model requires three separate programs in order to execute. Steps 1 through 3 (Figure 2) are executed in python (2.7, with the exception of step 2, which requires Python 3.x). After the flowpaths are prepped in Python, the volumes are produced in a R script which takes the mean (2830 m^3) and standard deviation (6190 m^3) of the field measured volumes to produce a log-normal distribution which can randomly sampled from for each simulated landslide (1 volume per flowpath produced) (Figure 8). The DFLOWZ simulations occur in a modified script of DFLOWZ (Berti and Simoni, 2007) within MATLAB. Modifications to DFLOWZ include adding FOR loops to various sections of the script in order to negate manually inputting each landslide. Additionally, corrections to the cross-sections normal to flow path were done in order to troubleshoot a bug in this section of the code. The resulting simulated runout for each landslide is added to a matrix that is ultimately converted to an ASCII file for importing to ArcGIS.

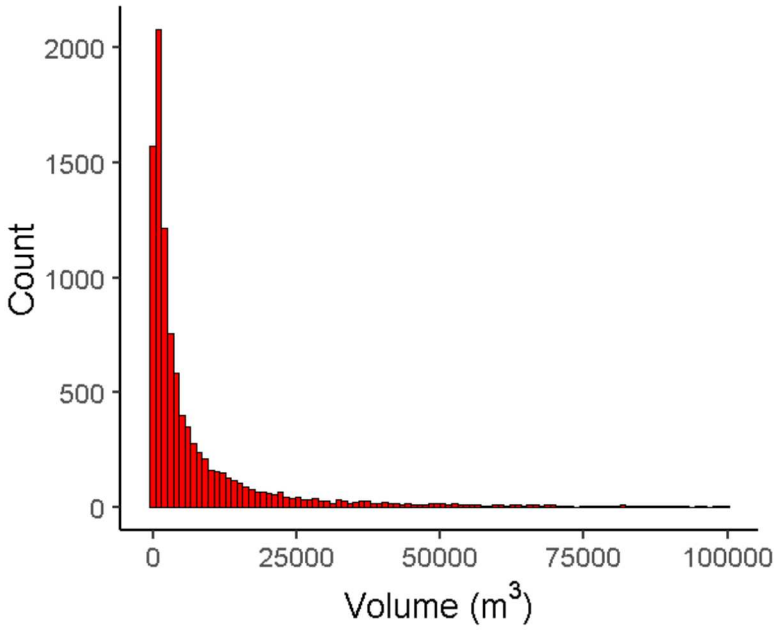

Figure 8. Log-normal distribution of debris flow volumes calibrated by field measured debris flows near Sitka.

Appendix D. Carbon models and landslide inventory

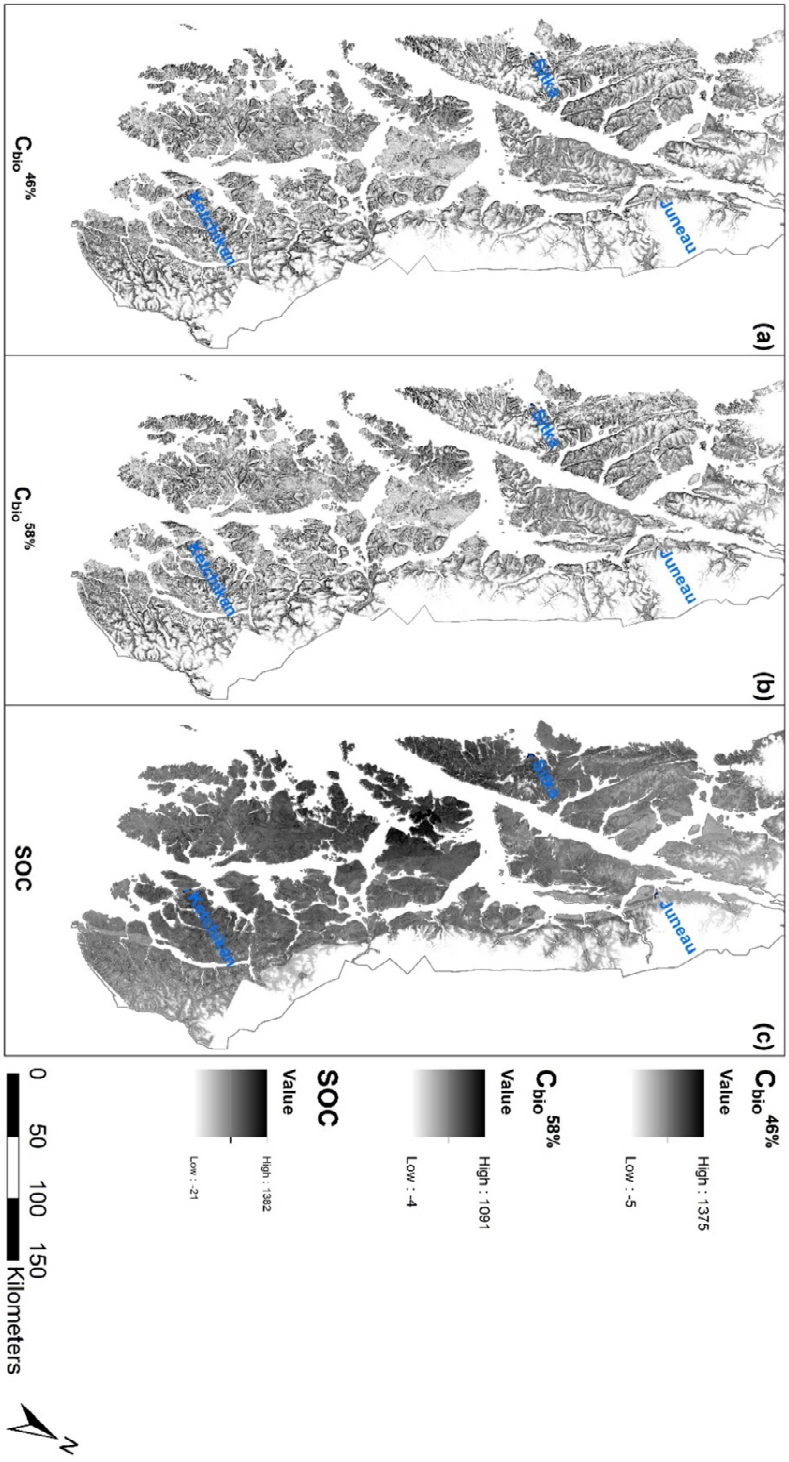

Figure 9. $C_{bio}^{46\%}$ and $C_{bio}^{58\%}$ scaled aboveground biomass carbon models from Buma & Thompson (2019) and the SOC model from McNicol et al. (2019) which were used in obtaining landslide mobilization rates.

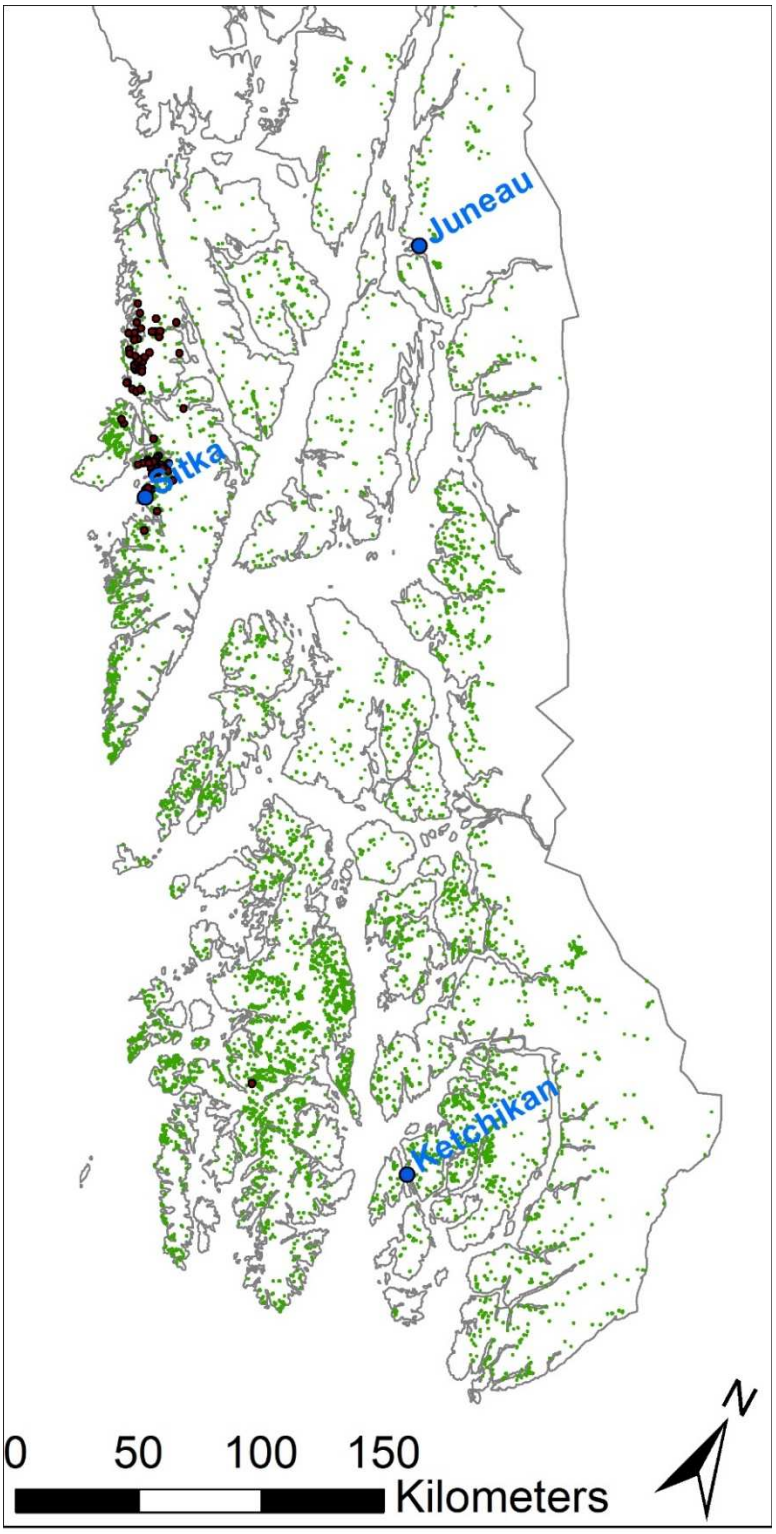

Figure 10. Landslide locations from the Tongass National Forest Landslide Inventory. Green points are debris flow classified landslides used in extracting carbon amounts from the respective models (Figure 8). Red points are debris flows triggered during the 2015 event.